

# ISOLATION OF CLERODIN FROM CLERODENDRUM INFORTUNATUM WITH THEORETICAL STUDIES (AIM AND DFT) OF CLERODIN (CLD) AND DEACETYLCLERODIN (DCLD)

<sup>1</sup>Sudha jain, <sup>1</sup>Ruchi verma, <sup>1</sup>Reetu sangwan, <sup>2</sup>Mohmmad Faheem Khan, <sup>1</sup>Monika sainsi Ashok kumar

<sup>1</sup>Department of Chemistry,  
University of Lucknow,  
Lucknow-226001, UP, India

<sup>2</sup>Department of Biotechnology,  
Era's Lucknow Medical College & Hospital, Era University  
Lucknow-226003, UP, India

**Abstract:** Clerodanes constitute an important class of natural products which exist in a various parts of terrestrial plants as well as marine sources. In present study, the isolation and purification of clerodin (CLD) from *Clerodendrum infortunatum* (family Verbenaceae), synthesis of deacetyclerodin (DCLD) derivative from clerodin (CLD) and a comparative analysis of CLD and DCLD has been performed using density functional theory (DFT) with B3LYP method and 6-311G (d, p) as the basis set. The optimized structures of both, natural compound and deacetyl derivative have been obtained. The vibrational spectroscopic analysis has been carried out and complete assignments to all possible modes have been offered. The highest occupied molecular orbital (HOMO), lowest unoccupied molecular orbital (LUMO) and molecular electrostatic potential (MESP) surfaces are analyzed to discuss the chemical reactivity patterns in the compounds. A number of reactivity parameters have also been calculated to further explain their chemical reactivity. The thermodynamic and nonlinear optical (NLO) parameters have also been calculated and discussed. For the theoretical detection and characterization of intramolecular hydrogen bonding within these compounds, QTAIM calculations have been done using AIMALL Program.

**Keywords:** Natural product chemistry, Theoretical chemistry, Organic chemistry

## 1. INTRODUCTION

Clerodanes constitute an important class of natural products isolated from various parts of terrestrial plants as well as marine sources.<sup>[1]</sup> The diterpenoid clerodin (CLD) has been isolated from *Clerodendrum infortunatum* (family Verbenaceae). In traditional medicines, the plant is widely used as blood purifier<sup>[2]</sup> and to cure common ailments viz. bronchitis, asthma, fever, inflammation<sup>[3]</sup>, tuberculosis, burning sensation, hepatoprotective<sup>[4]</sup>, antiepileptic<sup>[5,6,7]</sup>, colic pain, scorpion sting<sup>[8,9]</sup>, antidote for snakebite<sup>[10,11]</sup> and treatment of tumor<sup>[12]</sup>. The leaves and roots are also used as antidiabetic<sup>[13]</sup>. The plant extract also showed antimicrobial<sup>[14]</sup>, antioxidant<sup>[15]</sup> and ant-inflammatory activities<sup>[16]</sup>. In Unani system it was used against rheumatism and vermifugal.<sup>[17]</sup> Clerodin (CLD) has shown remarkably higher antifeedant activity than the commercially used ingredient azadirachtin when tested on a polyphagous pest, *Helicoverpa armigera*<sup>[18]</sup>. The comparative data showed that CLD could be an ingredient in the new biopesticides<sup>[19]</sup>. Further clerodin (CLD) has shown to possess growth inhibitory activity<sup>[20]</sup>. Clerodane diterpenoids have been reported pharmacophagous feeding stimulant activity<sup>[21]</sup>.

The present study describes the theoretical investigations on clerodin (CLD) and deacetyclerodin (DCLD) (prepared by deacetylation of clerodin) using density functional theory (DFT) and quantum theory of atoms-in-compound (QTAIM). theory (DFT) and quantum theory of atoms-in-compound (QTAIM). Recently, DFT has become a popular tool in computational chemistry and physics for evaluating the various chemical, physical, and biological phenomena featuring the realm of chemistry. For medium-sized chemical species<sup>[22-28]</sup> as well as biocompounds<sup>[29-31]</sup> DFT provides accurate results and a good balance between computational cost and perfection. The optimized structures, spectral studies, intra- and/or intermolecular interactions, kinetics and nature of chemical reactions can be easily and quickly identified with DFT, a quantum mechanical method. Unlike the wave function, which is a mathematical construct and not a physical reality, electron density is a physical diagnostic of all compounds. Our present study is based on the DFT (B3LYP functional and 6-31G (d,p) basis set) to successfully estimate a range of molecular properties (structural and electronic) and topological parameters based on the QTAIM technique. The investigation of the properties and reactivity of molecular structures is done with the help of The Bader<sup>[32,33]</sup> QTAIM method. The topological parameters viz. charge density at bond critical point ( $\rho_{BCP}$ ), potential energy density ( $V_{BCP}$ ), kinetic energy density ( $G_{BCP}$ ) and total energy density ( $H$ ) etc. are the basis of the very famous QTAIM theory. The aim of this work is to provide a brief description of the isolation of clerodin (CLD) and further modification of this compound to convert it in to chemically more reactive deacetyclerodin (DCLD) derivative to enhance its hydrophilic properties and biological activities. Along with this the theoretical characterization of weak intermolecular H---H, C---H and O---H bonding interactions are also discussed for CLD and DCLD. All the calculations of both the compound obtained from above mentioned theoretical methods are compared and reported. To our knowledge, this is the first report on these two compounds that deals with bonding interactions and chemical reactivity calculated from DFT methods and QTAIM analysis.

## 2.0. EXPERIMENTAL

### 2.1. General procedures

The Infrared (IR) spectra were measured on a Perkin-Elmer FTIR spectrophotometer. <sup>1</sup>H and <sup>13</sup>C NMR spectra (chemical shifts in ppm, coupling constants in Hz) were recorded on a Bruker 300 MHz using CDCl<sub>3</sub> as solvent, with TMS as the internal reference. The UV spectrum were determined using UV- visible Double-Beam Spectrophotometer (systronic-2203) instrument using chloroform as a solvent. Melting points were carried out using an Electrothermal Ambassador Melting Point apparatus. Column chromatographic separations were performed on SiO<sub>2</sub> (230-400 mesh). TLC was performed on pre-coated TLC plates with SiO<sub>2</sub> F<sub>254</sub> (0.2 mm, Merck). The solvent systems used for TLC analyses were n-hexane:EtOAc (60:40, **CLD**), n-hexane:EtOAc (60:40, **DCLD**). The Thin layer chromatography (TLC) was visualized in an iodine chamber. The compounds were detected by UV absorption at λ<sub>max</sub> 244 and 242 nm followed by spraying with anisaldehyde: H<sub>2</sub>SO<sub>4</sub> reagent and heating at 110 °C for 1–2 min.

### 2.2. Plant material

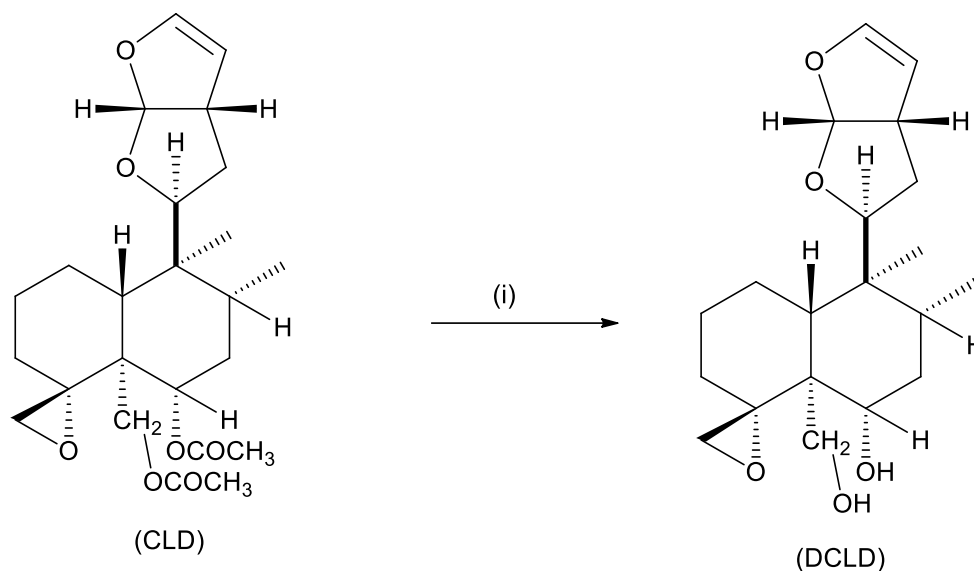
The floral parts of *Clerodendrum infortunatum* were collected from Lalpal Pur, Hardoi, Uttar Pradesh India (2.8 kg dry weight). The botanical authentication was established with the aid of taxonomists and treaties on regional flora comparison of specimens with herbaria by Botanical Survey of India Dehradun (BSD Accession No. 112672).

### 2.3. Extraction and isolation

The shade dried powdered floral parts (2.8 kg) were exhaustively extracted with 90% methanol at room temperature. The combined methanolic extract was concentrated under reduced pressure at 40° C to yield a dark viscous mass. It was concentrated to dryness, added water (100ml), extracted with hexane (3 x 1000 ml) and the hexane layer was washed with H<sub>2</sub>O, dried (anhyd.Na<sub>2</sub>SO<sub>4</sub>). Evaporation of the solvent under reduced pressure gave solid residue A (153.4 g). The residue A (153.4 g) was subjected to column chromatography over silica gel (459g,230-400 mesh column length 90 cm and radius 2 cm) the column was eluted with increasing polarity of solvent (Hexane, Hexane: EtOAc (3:1,1:1,1:3), EtOAc) and elutes were collected in fraction of 100 ml each, evaporated to dryness under reduced pressure. The eluant (Hexane: EtOAc) (85:15) fractions exhibiting similar TLC behavior were mixed together and rechromatographed which resulted in the isolation of pure compound as white needle shape crystals (1.5 gm); m. p. 160-162°C; IR (KBr; ν<sub>max</sub>, cm<sup>-1</sup>): 3140, 3040, 2956, 2936, 2930, 2931, 1736, 1731, 1625, 1288, 1272, 1238, 1051; <sup>1</sup>H (CDCl<sub>3</sub>, 300 MHz; δ, ppm): 1.04-1.90 m (12H, H1, H2, H3, H7, H8, H10, H12), 4.79 dd (1H, H6), 3.99 dd (1H, H11), 3.58 t (1H, H13), 4.91 d (1H, H14), 6.46 d (1H, H15), 5.99 d (1H,H16), 0.84 d (3H, H17), 2.20 d (1H, H18), 2.21 d (1H, H18b), 4.03 d (1H,H19a), 4.34 d (1H, H19b), 0.99 s (3H, H20), 1.90(s,3H,OAc), 2.17 (s,3H,OAc); <sup>13</sup>C (CDCl<sub>3</sub>, 75 MHz; δ, ppm): 22.35(C-1), 25.11(C-2), 31.33(C-3), 65.13(C-4), 45.65(C-5), 72.05(C-6), 32.83(C-7), 36.30(C-8), 40.14(C-9), 48.73(C-10), 84.71(C-11), 32.83(C-12), 46.12(C-13), 107.80(C-14), 146.97(C-15), 102.03(C-16), 14.24(C-17), 48.55(C-18), 61.83(C-19), 16.52(C-20), 170.02(O<sub>2</sub>C<sub>2</sub>H<sub>3</sub>), 171.12 (O<sub>2</sub>C<sub>2</sub>H<sub>3</sub>), 21.43 (OCO<sub>2</sub>H), 21.39 (OCO<sub>2</sub>H) **Fig S1** and **S2**. The compound was characterized as clerodin, (1R,4aR,5S,6R,8S,8aR)-8-acetoxy-5,6-dimethyl-5-((2S,3aS,6aS)-2,3,3a,6a-tetrahydrofuro[2,3-b]furan-2-yl)octahydro-2H-spiro[naphthalene-1,2'-oxiran]-8a-yl)methyl acetate) by comparison of the spectral data reported [65].

#### Synthesis of (1R,4aR,5S,6R,8S,8aR) -8a- (hydroxymethyl) -5,6-dimethyl-5- (2S,3aS,6aS)-2,3,3a,6a-tetrahydrofuro[2,3-b]furan-2-yl)octahydro-2H-spiro[naphthalene-1,2'-oxiran]-8-ol [deacetylclerodin (**DCLD**)]

In a round bottom flask **CLD** (100 mg, 4.34 mmol) was taken and added 3% methanolic potassium hydroxide solution (150 ml).The reaction mixture was stirred for 2 hrs at 0°C. The progress of the reaction was monitored by TLC. After completion of the reaction, the reaction mixture was cooled and solvent evaporated under reduced pressure, extracted with chloroform and dried (anhyd. Na<sub>2</sub>SO<sub>4</sub>). Deacetylclerodin (**DCLD**) (1R,4aR,5S,6R,8S,8aR)-8a-(hydroxymethyl)-5,6-dimethyl-5-((2S,3aS,6aS)-2,3,3a,6a-tetrahydrofuro[2,3-b]furan-2-yl)octahydro-2H-spiro[naphthalene-1,2'-oxiran]-8-ol,(**DCLD**) was obtained as white crystals<sup>[66]</sup>. yield: 87.3%; m.p. 170-172°C IR (KBr; ν<sub>max</sub>, cm<sup>-1</sup>) 3462 (OH), 3364 (OH), 2968, 2942, 1619, 1135, 1103, 1037, 998; <sup>1</sup>H (CDCl<sub>3</sub>, 300 MHz; δ, ppm): 1.13-1.97 (12H, H1, H2, H3, H7, H8, H10, H12), 4.07 dd (1H, H6), 3.59 dd (1H, H11), 2.08 t (1H, H13), 4.32 d (1H, H14), 6.45 d (1H, H15), 6.01 d (1H,H16), 0.97 d (3H, H17), 2.35 d (1H, H18), 2.50 d (1H, H18b), 4.02 d (1H,H19a), 4.10 d (1H, H19b), 1.09 s (3H, H20), 4.79 s (1H, OH), 3.16 s (1H,OH), <sup>13</sup>C (CDCl<sub>3</sub>, 75 MHz; δ, ppm): 22.94 (C-1), 25.35(C-2), 31.73(C-3), 74.43(C-4), 59.93(C-5), 75.81(C-6), 34.60(C-7), 36.40(C-8), 51.07(C-9), 47.74(C-10), 85.00(C-11), 31.73(C-12), 46.20(C-13), 102.10(C-14), 146.05(C-15), 107.94(C-16), 14.74(C-17), 48.31(C-18), 61.73(C-19), 16.99(C-20) **Fig S3** and **S4**.



Scheme 1: Synthesis of deacetylclerodin (DCLD) : (i) KOH, MeOH, 0°C, 2 hr

### 3. Computational details

The DFT calculations have been done with Gaussian 03 program package<sup>[34]</sup> and Gaussian 09 program package<sup>[35]</sup> and all theoretical analysis were done with the help of Gaussview 03 molecular visualization program<sup>[36]</sup> and Gaussview 5.0 molecular visualization program.<sup>[37]</sup> The investigation of optimized structural parameters, thermodynamic properties, vibrational assignments, HOMO–LUMO properties etc. were calculated using DFT<sup>[38-45]</sup> and TDDFT. A hybrid functional B3LYP which is described as B3<sup>[46]</sup> is becke's three parameter exchange (local, non local, Hartree–Fock) and LYP is Lee–Yang–Parr correlation functional.<sup>[47]</sup> All the calculations were done using 6-31G(d, p) basis set. All predictions of intramolecular hydrogen bonding were done using AIMALL program using QTAIM theory.

## 4. Results and Discussion

### 4.1 Molecular Structures

The optimized geometries of both the compounds at B3LYP /6-31G (d, p) level of theory are shown in **Fig. 1**. Both the compounds contain four ring system. Both rings R1 and R2 have same furan skeleton except that in **CLD** R1 ring has C=C bond between C21 and C22 whereas in derivative **DCLD** R1 has C=C bond between C25 and C26. In ring 4 i.e. R4 in **CLD** and **DCLD** compounds, oxirane ring are attached with the C7 and C3 positions respectively. In **CLD** two acetyl groups are attached at C3 and C11 (R3) positions while in its derivative **DCLD** these acetyl groups are replaced by two hydroxy groups (R3). In compound **CLD** R3 contains two methyl groups at C1 and C6 positions while in **DCLD** R3 contains two methyl groups at C9 and C10 positions. The calculated bond lengths and bond angles of both optimized structures are given in **Table 1**.

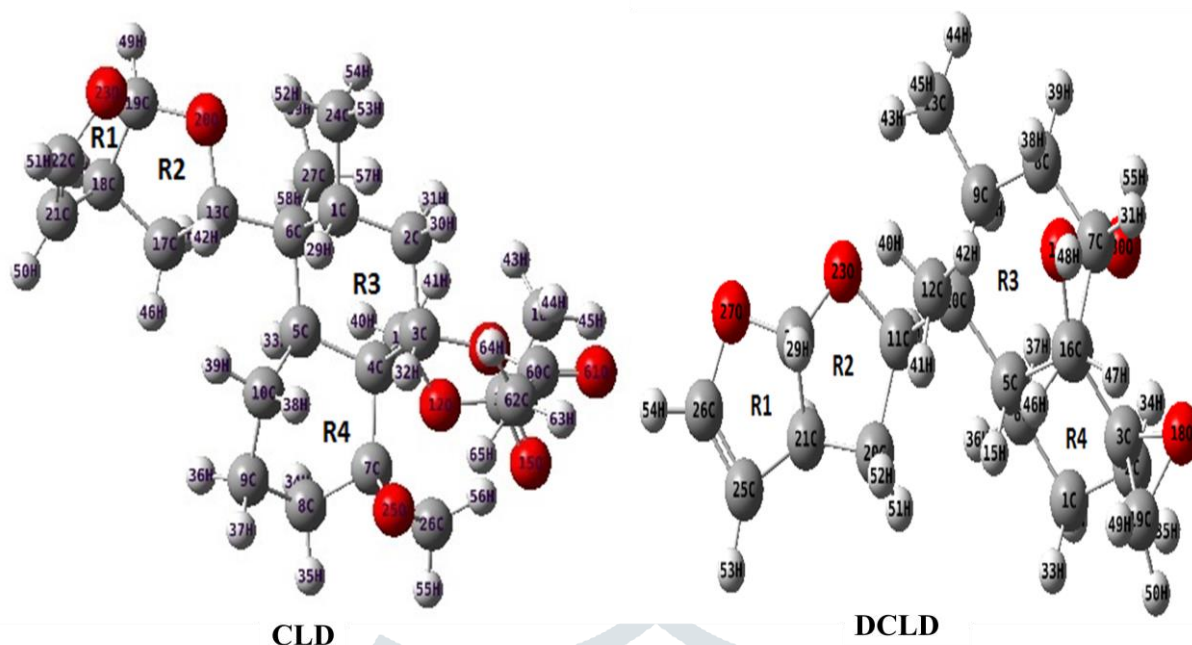


Fig 1. Optimized structure of CleroDin (CLD) and deacetylcleroDin derivative (DCLD)

Table 1. Geometrical parameters of optimized geometries of CLD and DCLD at B3LYP/6-31G (d, p) level

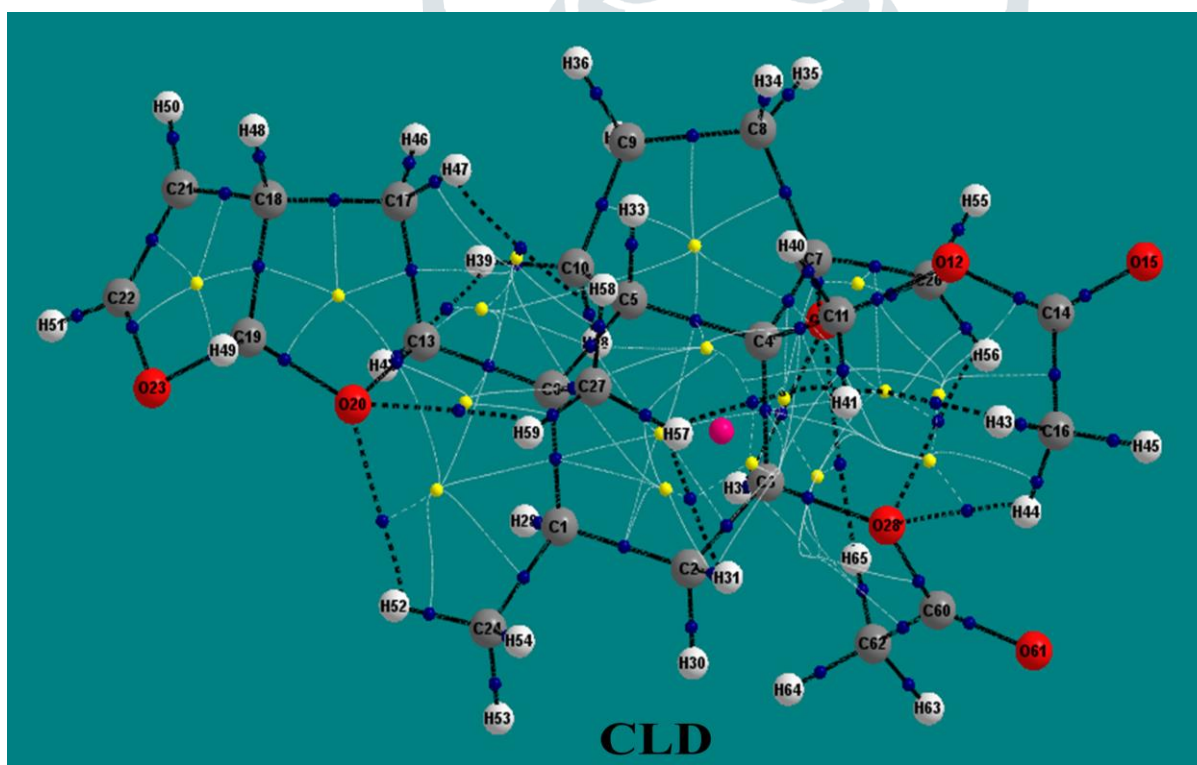
CLD		DCLD		DCLD		DCLD	
Bond -length (Å)		Bond -angle (°)		Bond -length (Å)		Bond -angle (°)	
R(1-2)	1.458	A(2-1-6)	104.3816	R(1-2)	1.5402	A(2-1-6)	109.4182
R(1-6)	1.5229	A(2-1-24)	110.7035	R(1-6)	1.5366	A(2-1-32)	109.5327
R(1-24)	1.523	A(2-1-29)	112.4165	R(1-32)	1.07	A(2-1-33)	109.4421
R(1-29)	1.113	A(6-1-24)	110.7099	R(1-33)	1.0699	A(6-1-32)	109.374
R(2-3)	1.523	A(6-1-29)	112.4258	R(2-3)	1.5428	A(6-1-33)	109.5966
R(2-30)	1.113	A(24-1-29)	106.301	R(2-34)	1.07	A(32-1-33)	109.4637
R(2-31)	1.113	A(1-2-3)	104.3798	R(2-35)	1.07	A(1-2-3)	109.7585
R(3-4)	1.523	A(1-2-30)	110.708	R(3-4)	1.5435	A(1-2-34)	109.4924
R(3-28)	1.402	A(1-2-31)	112.4244	R(3-18)	1.5127	A(1-2-35)	109.2856
R(3-32)	1.1131	A(3-2-30)	110.7071	R(3-19)	1.424	A(3-2-34)	109.5266
R(4-5)	1.5229	A(3-2-31)	112.4215	R(4-5)	1.5398	A(3-2-35)	109.2523
R(4-7)	1.505	A(30-2-31)	106.2976	R(4-7)	1.5398	A(34-2-35)	109.5114
R(4-11)	1.523	A(2-3-4)	109.4727	R(4-16)	1.54	A(2-3-4)	107.788
R(5-6)	1.5229	A(2-3-28)	109.4503	R(5-6)	1.5372	A(2-3-18)	116.0626
R(5-10)	1.523	A(2-3-32)	109.4826	R(5-10)	1.5396	A(2-3-19)	119.2656
R(5-33)	1.113	A(4-3-28)	109.4494	R(5-15)	1.07	A(4-3-18)	122.9992
R(6-13)	1.523	A(4-3-32)	109.4768	R(6-36)	1.07	A(4-3-19)	121.4307
R(6-27)	1.523	A(28-3-32)	109.4955	R(6-37)	1.07	A(3-4-5)	109.7998
R(7-8)	1.505	A(3-4-5)	109.4689	R(7-8)	1.5406	A(3-4-7)	109.6142
R(7-25)	1.435	A(3-4-7)	112.4016	R(7-30)	1.43	A(3-4-16)	109.1818
R(7-26)	1.467	A(3-4-11)	108.5112	R(7-31)	1.07	A(5-4-7)	109.3446
R(8-9)	1.5942	A(5-4-7)	112.4017	R(8-9)	1.5401	A(5-4-16)	109.409
R(8-34)	1.113	A(5-4-11)	108.5139	R(8-38)	1.07	A(7-4-16)	109.4776
R(8-35)	1.113	A(7-4-11)	105.3332	R(8-39)	1.07	A(4-5-6)	109.3891
R(9-10)	1.523	A(4-5-6)	109.4725	R(9-10)	1.5401	A(4-5-10)	109.5169
R(9-36)	1.113	A(4-5-10)	109.471	R(9-13)	1.54	A(4-5-15)	109.4483
R(9-37)	1.113	A(4-5-33)	109.4741	R(9-14)	1.07	A(6-5-10)	109.2678
R(10-38)	1.113	A(6-5-10)	109.4679	R(10-11)	1.5401	A(6-5-15)	109.6655
R(10-39)	1.113	A(6-5-33)	109.4735	R(10-12)	1.54	A(10-5-15)	109.5396
R(11-12)	1.402	A(10-5-33)	109.4682	R(11-20)	1.5644	A(1-6-5)	109.4377
R(11-40)	1.113	A(1-6-5)	109.4729	R(11-23)	1.5065	A(1-6-36)	109.5693
R(11-41)	1.1129	A(1-6-13)	109.4497	R(11-24)	1.07	A(1-6-37)	109.3939
R(12-14)	1.338	A(1-6-27)	109.4775	R(12-40)	1.07	A(5-6-36)	109.5595
R(13-17)	1.5229	A(5-6-13)	109.4528	R(12-41)	1.07	A(5-6-37)	109.4018
R(13-20)	1.3767	A(5-6-27)	109.4783	R(12-42)	1.07	A(36-6-37)	109.465
R(13-42)	1.113	A(13-6-27)	109.4961	R(13-43)	1.07	A(4-7-8)	109.4162
R(14-15)	1.208	A(4-7-8)	119.9998	R(13-44)	1.07	A(4-7-30)	109.4879
R(14-16)	1.5091	A(4-7-25)	115.0015	R(13-45)	1.07	A(4-7-31)	109.486

R(16-43)	1.113	A(4-7-26)	118.2002	R(16-17)	1.43	A(8-7-30)	109.5307
R(16-44)	1.113	A(8-7-25)	114.9954	R(16-46)	1.07	A(8-7-31)	109.4438
R(16-45)	1.113	A(8-7-26)	118.2018	R(16-47)	1.07	A(30-7-31)	109.4627
R(17-18)	1.523	A(7-8-9)	117.0201	R(17-48)	0.96	A(7-8-9)	109.5331
R(17-46)	1.113	A(7-8-34)	107.5305	R(18-19)	1.5615	A(7-8-38)	109.4404
R(17-47)	1.113	A(7-8-35)	105.0537	R(19-49)	1.07	A(7-8-39)	109.4679
R(18-19)	1.5231	A(9-8-34)	107.5297	R(19-50)	1.07	A(9-8-38)	109.4426
R(18-21)	1.497	A(9-8-35)	105.0502	R(20-21)	1.4602	A(9-8-39)	109.4629
R(18-48)	1.113	A(34-8-35)	114.9727	R(20-51)	1.07	A(38-8-39)	109.4805
R(19-20)	1.402	A(8-9-10)	115.3074	R(20-52)	1.07	A(8-9-10)	109.4985
R(19-23)	1.414	A(8-9-36)	107.9759	R(21-22)	1.4556	A(8-9-13)	109.4728
R(19-49)	1.1129	A(8-9-37)	106.0557	R(21-25)	1.4863	A(8-9-14)	109.4522
R(21-22)	1.337	A(10-9-36)	107.969	R(21-28)	1.07	A(10-9-13)	109.4712
R(21-50)	1.1	A(10-9-37)	106.0579	R(22-23)	1.4353	A(10-9-14)	109.4517
R(22-23)	1.4202	A(36-9-37)	113.6522	R(22-27)	1.4344	A(13-9-14)	109.4809
R(22-51)	1.0999	A(5-10-9)	109.4701	R(22-29)	1.07	A(5-10-9)	109.3562
R(24-52)	1.113	A(5-10-38)	109.4525	R(25-26)	1.3885	A(5-10-11)	109.5197
R(24-53)	1.1129	A(5-10-39)	109.4813	R(25-53)	1.07	A(5-10-12)	109.5096
R(24-54)	1.113	A(9-10-38)	109.445	R(26-27)	1.5004	A(9-10-11)	109.4618
R(25-26)	1.2583	A(9-10-39)	109.4758	R(26-54)	1.07	A(9-10-12)	109.53
R(26-55)	1.087	A(38-10-39)	109.502	R(30-55)	0.96	A(11-10-12)	109.4501
R(26-56)	1.087	A(4-11-12)	109.5001			A(10-11-20)	108.2425
R(27-57)	1.113	A(4-11-40)	109.4401			A(10-11-23)	114.8595
R(27-58)	1.1131	A(4-11-41)	109.4614			A(10-11-24)	108.9919
R(27-59)	1.113	A(12-11-40)	109.4415			A(20-11-23)	105.2409
R(28-60)	1.338	A(12-11-41)	109.4649			A(20-11-24)	112.9669
R(60-61)	1.208	A(40-11-41)	109.5193			A(23-11-24)	106.6226
R(60-62)	1.509	A(11-12-14)	109.8998			A(10-12-40)	109.4694
R(62-63)	1.113	A(6-13-17)	111.5477			A(10-12-41)	109.4733
R(62-64)	1.113	A(6-13-20)	111.549			A(10-12-42)	109.4718
R(62-65)	1.113	A(6-13-42)	104.3131			A(40-12-41)	109.4724
		A(17-13-20)	100.8947			A(40-12-42)	109.4685
		A(17-13-42)	114.408			A(41-12-42)	109.472
		A(20-13-42)	114.4094			A(9-13-43)	109.4715
		A(12-14-15)	120.0025			A(9-13-44)	109.4733
		A(12-14-16)	119.9998			A(9-13-45)	109.4674
		A(15-14-16)	119.9977			A(43-13-44)	109.4721
		A(14-16-43)	109.4988			A(43-13-45)	109.4706
		A(14-16-44)	109.4407			A(44-13-45)	109.4724
		A(14-16-45)	109.4605			A(4-16-17)	109.4773
		A(43-16-44)	109.4434			A(4-16-46)	109.466
		A(43-16-45)	109.4629			A(4-16-47)	109.47
		A(44-16-45)	109.521			A(17-16-46)	109.4731
		A(13-17-18)	104.0008			A(17-16-47)	109.4703
		A(13-17-46)	110.8028			A(46-16-47)	109.4706
		A(13-17-47)	112.6414			A(16-17-48)	109.4698
		A(18-17-46)	110.7976			A(3-19-49)	119.6937
		A(18-17-47)	112.6381			A(3-19-50)	121.3775
		A(46-17-47)	106.0742			A(18-19-49)	116.3207
		A(17-18-19)	103.9986			A(18-19-50)	123.1023
		A(17-18-21)	109.467			A(49-19-50)	108.8628
		A(17-18-48)	111.3158			A(11-20-21)	97.6398
		A(19-18-21)	104.0018			A(11-20-51)	115.4141
		A(19-18-48)	116.2105			A(11-20-52)	110.0533
		A(21-18-48)	111.3143			A(21-20-51)	117.9935
		A(18-19-20)	103.9948			A(21-20-52)	107.4898
		A(18-19-23)	103.9943			A(51-20-52)	107.7245
		A(18-19-49)	116.2182			A(20-21-22)	98.1652
		A(20-19-23)	109.5014			A(20-21-25)	122.6253
		A(20-19-49)	111.3021			A(20-21-28)	110.1705
		A(23-19-49)	111.3009			A(22-21-25)	102.1617
		A(13-20-19)	111.9009			A(22-21-28)	115.5444
		A(18-21-22)	111.001			A(25-21-28)	107.9803
		A(18-21-50)	124.5052			A(21-22-23)	102.9375
		A(22-21-50)	124.4939			A(21-22-27)	103.8554
		A(21-22-23)	108.1004			A(21-22-29)	112.31
		A(21-22-51)	125.9494			A(23-22-27)	121.079

A(23-22-51)	125.9502
A(19-23-22)	112.5862
A(1-24-52)	109.4961
A(1-24-53)	109.4416
A(1-24-54)	109.4573
A(52-24-53)	109.4434
A(52-24-54)	109.4629
A(53-24-54)	109.526
A(7-26-55)	119.4526
A(7-26-56)	133.6881

## 4.2 Hydrogen Bonding

For the theoretical detection and characterization of intramolecular hydrogen bonding within these compounds, the *QTAIM* calculations have been done using *AIMALL* Program. The bond critical point (*BCP*) between a proton donor and proton acceptor defines the hydrogen bonding in *QTAIM* framework. The chemical features of the molecule<sup>[48]</sup> is represented by the parameters of *BCP* viz. second order derivative of the electron density, the Laplacian ( $\nabla^2_{\rho BCP}$ ), charge density ( $\rho_{BCP}$ ), potential energy density ( $V_{BCP}$ ), kinetic energy density ( $G_{BCP}$ ), total energy density ( $H$ ) and energy of interaction ( $E$ ). The value of electron density ( $\nabla^2_{\rho BCP}$ ) can describe about the nature of hydrogen bonds in compound i.e.  $\nabla^2_{\rho BCP} < 0$  and  $\rho_{BCP} > 0$  atomic unit (au).<sup>[49]</sup> For charge concentrated in covalent (shared) interaction  $\nabla^2_{\rho BCP} > 0$  and  $H > 0$ , indicates that the hydrogen bonds are weak and electrostatic in nature. In our study it was found that **CLD** showed total eleven types of hydrogen bonding interactions. Out of which four are of H---H type weak interactions (H41---H57, H31---H57, H47---H58, H42---H39), one is of C---H type (C16---H41) and six are of H---O type interactions (H52---O20, H59---O20, O28---H56, O28---H44, O25---H65, O25---H32) while the **DCLD** showed total 12 types of hydrogen bonding interactions i.e. five are the H---H type weak interactions (H41---H52, H51---H36, H24---H36, H14---H37, H47---H49) and seven are of C-H---O type interactions (O23---H43, O23---H40, O17---H42, O18---H47, O30---H37, O30---H34, O17---H38). The bonding interactions in both the compounds are displayed in **Fig. 2**. The theoretical values of topological parameters are listed in **Table 2** for **CLD** and **DCLD**.



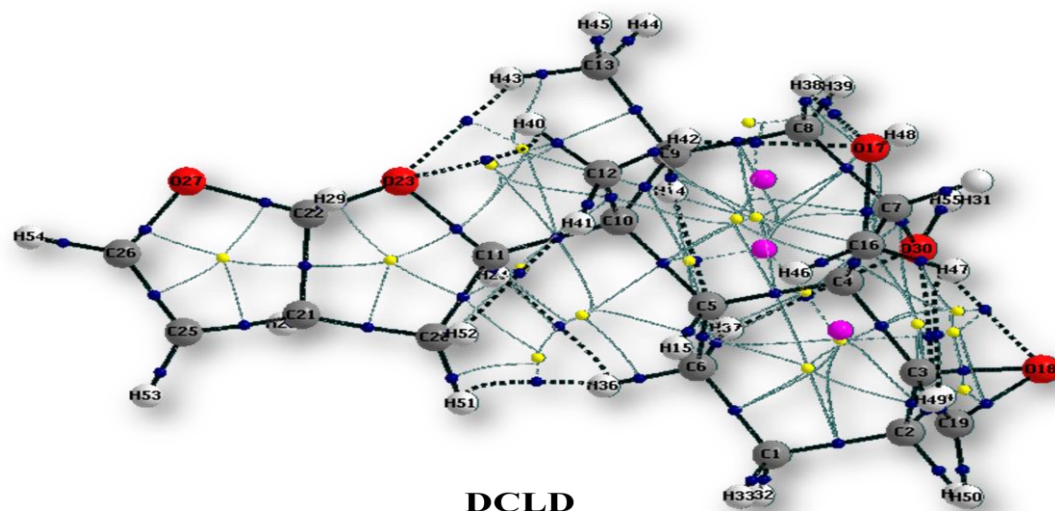


**Fig. 2.** Molecular graphs showing H---H, C---H, O---H intramolecular interactions (black dotted lines) in **CLD** and **DCLD**. The yellow points correspond to ring critical points, the blue points represent BCPs, the pink points correspond to CCPs and white lines correspond to RCPs to BCPs path. Red spheres correspond to oxygen atoms, dark grey spheres correspond to carbon atoms, and white spheres correspond to hydrogen atoms.

According to the Espinosa correlation<sup>[50]</sup> the *QTAIM* theory is also able to investigate the interaction energy of H-Bond as

$$E \text{ (au)} = 1/2 V_{BCP} \text{ (au)} = 313.754 V_{BCP} \text{ (kcal mol}^{-1}\text{)} = E \text{ (kcal mol}^{-1}\text{)} \quad (1)$$

where  $V_{BCP}$  is the potential energy density and  $E$  is the energy of interatomic interaction (a.u. or kcal mol<sup>-1</sup>), which can be easily calculated using the *AIMAll* package. **Table 2** showed that interaction energy,  $E$ , at their critical points, H52---O20 ( $E = 3.38384$  kcal mol<sup>-1</sup>), H59---O20 ( $E = 3.98593$  kcal mol<sup>-1</sup>) and O25---H32 ( $E = 4.48135$  kcal mol<sup>-1</sup>), these H-bonds are stronger than the other H-bonds of the **CLD** compound. **Table 2** also showed that interaction energy,  $E$ , at their critical points, O23---H43 ( $E = 3.51655$  kcal mol<sup>-1</sup>), O23---H40 ( $E = 3.79203$  kcal mol<sup>-1</sup>), O17---H42 ( $E = 5.94281$  kcal mol<sup>-1</sup>), O18---H47 ( $E = 4.99245$  kcal mol<sup>-1</sup>), H47---H49 ( $E = 3.9784$  kcal mol<sup>-1</sup>), O30---H34 ( $E = 4.69721$  kcal mol<sup>-1</sup>), O17---H38 ( $E = 4.59022$  kcal mol<sup>-1</sup>), the H-bonds are stronger than the other H-bonds of the **DCLD** compound. The Total interaction energy of **CLD** is 28.91619 kcal mol<sup>-1</sup> and **DCLD** is 42.7948 kcal mol<sup>-1</sup>. Thus, these studies shows that **DCLD** has higher values of interaction energy,  $E$  than **CLD** itself so it is clear that **DCLD** derivative is chemically more reactive as compared to **CLD**.

**Table 2.** Topological value of **CLD** and **DCLD** at B3LYP/6-31G (d, p) level

CLD								
Interactions	$\rho_{BCP}$	$\nabla^2\rho_{BCP}$	$G_{BCP}$	$V_{BCP}$	$H_{BCP}$	$E$	$BPL$	$ V(r) /G(r)$
H52---O20	+0.014677	+0.051915	+0.011882	-0.010785	-0.001472	3.38384	+4.471044	0.9076754
H59---O20	+0.016386	+0.068263	+0.014885	-0.012704	-0.001823	3.98593	+4.598471	0.8534766
H31---H57	+0.011309	+0.044955	+0.008834	-0.006429	-0.000204	2.01712	+4.205951	0.7277563
H41---H57	+0.010163	+0.040538	+0.007872	-0.005610	-0.000048	1.76016	+4.336552	0.7126524
H47---H58	+0.008760	+0.035622	+0.006802	-0.004700	-0.000127	1.47464	+0.008760	0.6909732
C16---H41	+0.013194	+0.060383	+0.012090	-0.009085	-0.000704	2.85046	+4.795034	0.7514474
O28---H56	+0.012327	+0.044843	+0.010024	-0.008837	-0.001185	2.77264	+4.649732	0.8815841
O28---H44	+0.008804	+0.031271	+0.006859	-0.005899	-0.000861	1.85083	+4.840128	0.8600379
O25---H65	+0.007614	+0.027173	+0.005880	-0.004967	-0.000638	1.55842	+5.019669	0.8447278
O25---H32	+0.018251	+0.072908	+0.016255	-0.014283	-0.002027	4.48135	+4.530271	0.8786834
H42---H39	+0.014087	+0.058286	+0.011717	-0.008863	-0.000560	2.7808	+4.158759	0.7564222
DCLD								
Interactions	$\rho_{BCP}$	$\nabla^2\rho_{BCP}$	$G_{BCP}$	$V_{BCP}$	$H_{BCP}$	$E$	$BPL$	$ V(r) /G(r)$
O23---H43	+0.015001	+0.054757	+0.012448	-0.011208	-0.001425	3.51655	+4.407932	0.9003856
O23---H40	+0.015543	+0.065503	+0.014231	-0.012086	-0.002053	3.79203	+4.813584	0.8492727
H41---H52	+0.009246	+0.037060	+0.007122	-0.004979	-0.000145	1.56218	+4.475204	0.6991013
H51---H36	+0.011145	+0.043458	+0.008662	-0.006459	-0.000300	2.02654	+4.192476	0.7456707
H24---H36	+0.014427	+0.063397	+0.012556	-0.009262	-0.000710	2.90599	+4.350124	0.7376553
H14---H37	+0.010723	+0.042382	+0.008348	-0.006101	-0.000149	1.91421	+4.227087	0.7308337
O17---H42	+0.023626	+0.067726	+0.017936	-0.018941	-0.001965	5.94281	+3.974406	1.056032
O18---H47	+0.019475	+0.075177	+0.017353	-0.015912	-0.001835	4.99245	+4.264514	0.9169596
H47---H49	+0.017074	+0.083490	+0.016776	-0.012680	-0.001485	3.9784	+4.401621	0.7558416
O30---H37	+0.012611	+0.043747	+0.010052	-0.009167	-0.001409	2.87618	+4.644721	0.9119578
O30---H34	+0.019192	+0.066657	+0.015818	-0.014971	-0.002044	4.69721	+4.196528	0.9464534
O17---H38	+0.018713	+0.067060	+0.015698	-0.014630	-0.001879	4.59022	+4.210902	0.9319658

### 4.3 HOMO - LUMO and MESP Surface

Frontier molecular orbitals play an important role in the investigation of the electronic transitions and chemical reactivity of a compound. These molecular orbitals involve HOMO and LUMO which takes part in chemical reactions or interact with other compounds. Intramolecular charge transfer within a molecule is related with HOMO-LUMO energy gap which can help to investigate the chemical and biological reactivity of the molecule. Since electron transfer occurs from HOMO to LUMO, the energy gap becomes an important measure for excitation energy, chemical hardness, molecular stability as the value of all these parameters will be low if the HOMO-LUMO energy gap is low. The HOMO-LUMO energy gap is an important stability index which reflects the chemical stability of the molecule. The energy gap diagrams of both the compounds are shown in **Fig. 3**. It is clearly seen that HOMOs of CLD and DCLD compounds are delocalized over ring R1 and R2 while in **CLD** LUMOs are delocalized in  $-\text{OCOCH}_3$  group attached to ring R3 and group  $-\text{CH}_2\text{OCOCH}_3$  attached at bridge head carbon of ring R3 and R4 while in its derivative LUMOs are contributed to only ring R1. The value of energy gap is 6.14 eV and 11.27 eV in **CLD** and **DCLD** respectively. The higher value HOMO-LUMO energy gap in **DCLD** indicates that its chemical reactivity is more than that of **CLD** as predicted earlier by increased hydrogen bonding.

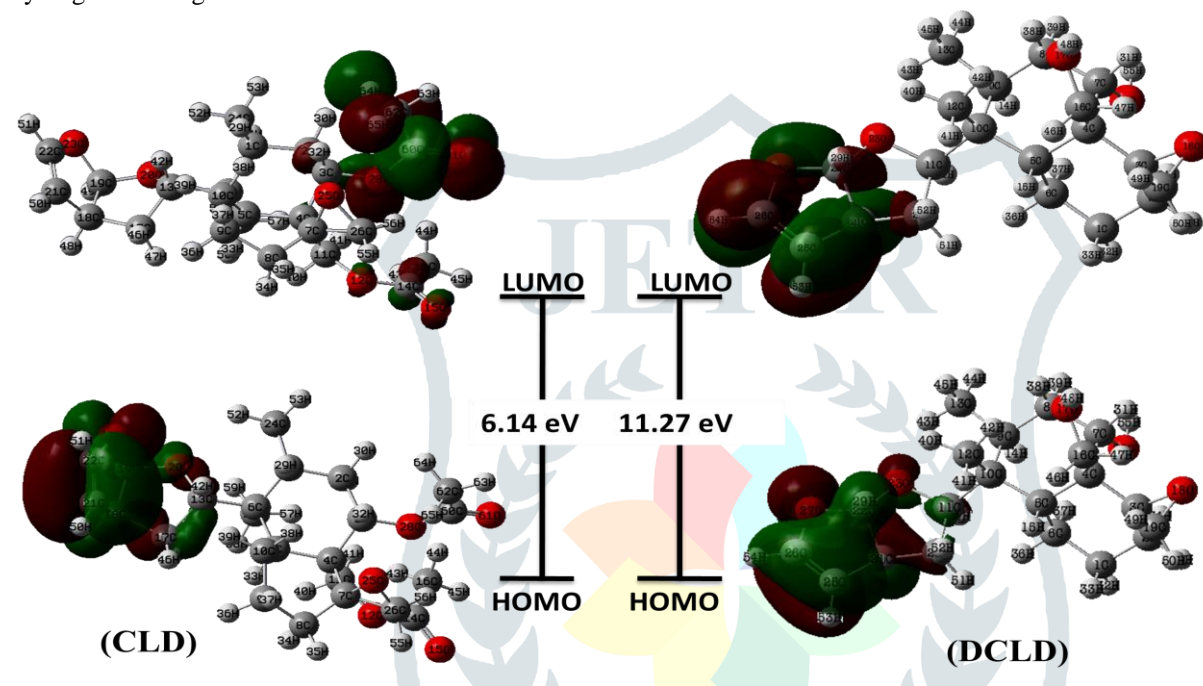


**Fig. 3.** HOMO –LUMO surface of **CLD** and **DCLD**

The mapping of constant electron density of compound is done with the help of molecular electrostatic potential (MESP) surface. It can help us to describe the shape, size, reactive sites for electrophilic attack (electron rich region), and nucleophilic attack (electron poor region) in term of color grading system which is an important tool for the investigation of most probable binding receptor site. The MESP plot of **CLD** and **DCLD** are displayed in **Fig. 4**. In color grading system, the blue color represents the most electropositive region which is C atom ( $-\text{OCOCH}_3$  group) in **CLD** and hydrogen attached to oxygen ( $-\text{OH}$  group) in **DCLD**. The red color represents the most electronegative region i.e. oxygen atom in ring R1 and R2 in both the compounds, O15, O61 and O25 in **CLD** and O30, O17 and O18 in **DCLD**.

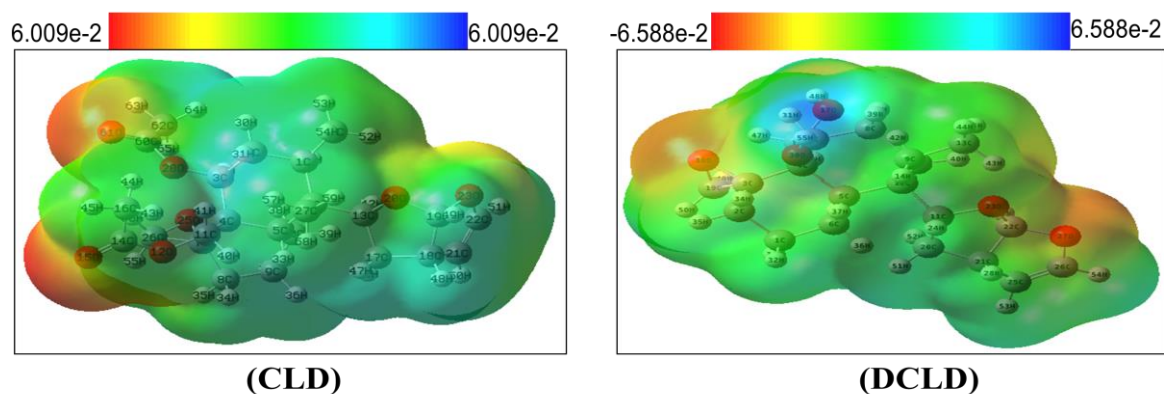


**Fig. 4.** MESP surface diagram of **CLD** and **DCLD**

#### 4.4 Electronic and Thermodynamic Parameters

The electronic parameters *viz.* energy band gap ( $\epsilon_{LUMO} - \epsilon_{HOMO}$ ), ionization potential ( $IP$ ), electron affinity ( $EA$ ), electronegativity ( $\chi$ ), global hardness ( $\eta$ ), chemical potential ( $\mu$ ) and global electrophilicity index ( $\omega$ ), global softness ( $S$ ) and additional electronic charge ( $\Delta N_{max}$ ) have been calculated at B3LYP/6-31G(d, p) level for **CLD** and **DCLD**. These electronic parameters are also called *global reactivity descriptors*. All these parameters are related to the chemical reactivity of compound. The electronic parameters of **r** are listed in **Table 3**. These calculations have been calculated using following equations. <sup>[42-58]</sup>

$$IP = -\epsilon_{HOMO} \quad (2)$$

$$EA = -\epsilon_{LUMO} \quad (3)$$

$$\chi = -1/2(\epsilon_{LUMO} + \epsilon_{HOMO}) \quad (4)$$

$$\eta = 1/2(\epsilon_{LUMO} - \epsilon_{HOMO}) \quad (5)$$

$$\mu = -\chi = 1/2(\epsilon_{LUMO} + \epsilon_{HOMO}) \quad (6)$$

$$\omega = \mu^2 / 2\eta \quad (7)$$

$$S = 1/2\eta \quad (8)$$

$$\Delta N_{max} = -\mu / \eta \quad (9)$$

It is clear from the **Table 3** that the value of  $I$  and  $A$  is lower for **CLD** in comparison to values of  $I$  and  $A$  of **DCLD** hence **CLD** has less electronegativity. However **CLD** is chemically less hard than its derivative **DCLD**.

**Table 3.** Calculated electronic parameters in eV for **CLD** and **DCLD** using B3LYP/6-31G (d,p)

	$\epsilon_H$	$\epsilon_L$	$\epsilon_H - \epsilon_L$	$I$	$A$	$\chi$	$H$	$\mu$	$\omega$	$S$	$\Delta N_{max}$
<b>CLD</b>	-6.016	0.133	-6.149	6.016	0.133	2.941	3.074	-2.941	1.407	0.1626	0.956
<b>DCLD</b>	-6.060	0.521	-6.581	6.060	0.521	2.769	3.290	-2.769	1.165	0.151	0.841

Thermodynamic parameters of **CLD** and **DCLD** *viz.* heat capacity (CV), entropy (S), zero point vibrational energy and total energy  $E_{total}$  etc. at B3LYP/6-31G(d, p) level are listed in **Table 4 and 5** respectively. Thermodynamic functions, heat capacity (CV) and entropy (S) were calculated at various temperatures (100-500 K) for both compounds. It was observed from **Fig. 5** that standard statistical thermodynamic functions increase with temperature ranging from 100 to 500 K, due to the fact that the molecular vibrational intensities increase with temperature. <sup>[59, 60]</sup> All thermodynamic calculations were done in gas phase and they could not be used in solution. All data of thermodynamic parameters are useful in estimating reaction paths of the compound. The correlation graph of entropy and heat capacity versus temperature is shown in **Fig. 5**.

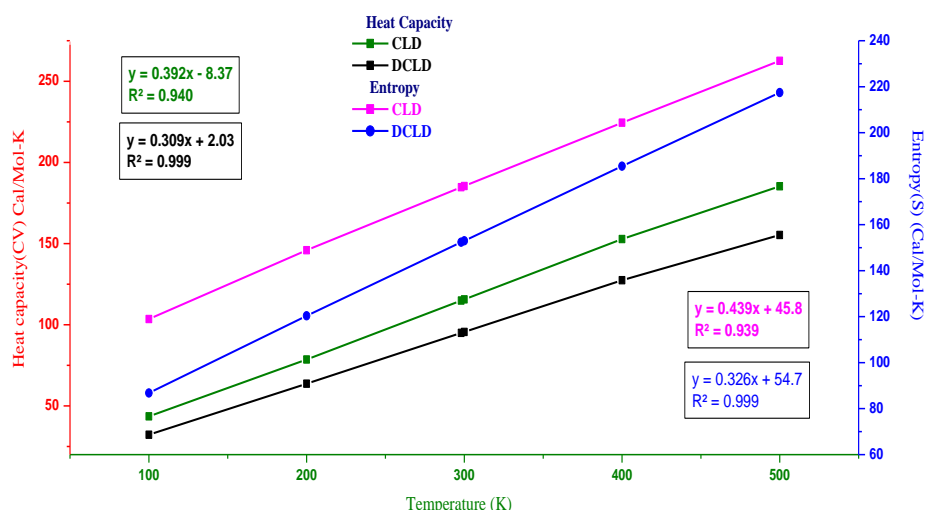


**Fig. 5.** Correlation graph of entropy and heat capacity versus temperature

**Table 4.** Thermodynamic functions at different temperatures at the B3LYP /6-31-G (d,p) level

Temperature (K)	Heat capacity (CV) (Cal/Mol-K)		Entropy (S) (Cal/Mol-K)	
	CLD	DCLD	CLD	DCLD
100	43.550	32.256	103.486	86.791
200	78.591	63.690	145.912	120.376
298	114.926	94.993	184.756	152.361
300	115.632	95.599	185.482	152.963
400	152.787	127.453	224.476	185.460
500	185.328	155.303	262.615	217.427

**Table 5.** Calculated Thermodynamic parameters

Parameters	B3LYP 6-31G (d,p)	
	CLD	DCLD
Zero point vibrational Energy (kcal/mol)	350.21176	302.82401
Rotational temperature (K)		
X	0.01331	0.02058
Y	0.00431	0.00677
Z	0.00412	0.00617
Rotational constant (GHZ)		
X	0.27739	0.42879
Y	0.08972	0.14097
Z	0.08581	0.12865
Total energy $E_{total}$ (kcal/mol)	368.214	317.089
Translational	0.889	0.889
Rotational	0.889	0.889
Vibrational	366.437	315.312

#### 4.5 Natural Bond Orbital Analysis

The Natural Bond Orbital (NBO) analysis were performed using Gaussian03 package at the B3LYP/6-31G (d, p) level of theory. This study offers the theoretical analysis of inter/intramolecular bonding, charge transfer, conjugative interaction in compound. The stabilization energy of the system is the basic concept for NBO analysis as if any molecular system bears high stabilization energy then the interaction between bonds will be high and high will be the conjugation. This means that the tendency of donating an electron from donor to acceptor will increase. NBO is found to be a great tool to explain the hyperconjugative interaction and electron density transfer. The second order Fock matrix was used to evaluate donor (i)-acceptor (j) interaction i.e. interaction between donor level bonds and acceptor level bonds in the NBO analysis. For each donor (i) and acceptor (j) the stabilization energy  $E(2)$  associated with the delocalization  $i \rightarrow j$  is as follows:

$$E(2) = \Delta E_{ij} = q_i(F_{ij})^2 / (E_j - E_i) \quad (10)$$

Where  $q_i$  is the donor orbital occupancy,  $E_i$  and  $E_j$  are the diagonal elements and  $F_{ij}$  is the off diagonal NBO Fock matrix element. The values of the stabilization energy  $E(2)$  along with other important parameters are shown in **Table 6**. According to the Table it is clearly predictable that increased electron density (ED) and intramolecular charge transfer (ICT) leads to the stabilization of the system in many bonding interactions. For the **CLD** system the most stabilization energy is contributed by O12 of  $n_2(O12)$  to C14-O15 with ED (0.20319 e) and stabilization energy  $E(2)$  is 42.91, O15 of  $n_2(O15)$  to O12-C14 with ED (0.11177 e) and stabilization energy  $E(2)$  is 35.87, O23 of  $n_2(O23)$  to C21-C22 with ED (0.14082 e) and stabilization energy  $E(2)$  is 31.04, O28 of  $n_2(O28)$  to C60-O61 with ED (0.20037 e) and stabilization energy  $E(2)$  is 39.92, O O61 of  $n_2(O61)$  to O28-C60 with ED (0.10921 e) and stabilization energy  $E(2)$  is 35.28. For the **DCLD** system the most stabilization energy is contributed by O27 of  $n_2(O27)$  to C25 - C26 with ED (0.12391 e) and stabilization energy  $E(2)$  is 23.83.

Table 6. NBO analysis of the CLD and DCLD

CLD								
Donor(i)	Type	ED/e	Acceptor(j)	Type	ED/e	E(2) <sup>a</sup>	E(j)-E(i) <sup>b</sup>	F(i,j) <sup>c</sup>
C7-O25	σ	1.97128	O25-C26	σ*	0.02351	5.47	0.93	0.064
O25-C26	σ	1.97661	C7-O25	σ*	0.05180	5.92	0.90	0.065
LP(1)O12	n	1.95572	C14-C16	σ*	0.05943	6.65	0.91	0.070
LP(2)O12	n	1.80427	C4-C11	σ*	0.03706	5.00	0.64	0.053
LP(2)O12	n	1.80427	C14-O15	π*	0.20319	<b>42.91</b>	0.34	0.108
LP(2)O15	n	1.84465	O12-C14	σ*	0.11177	<b>35.87</b>	0.61	0.133
LP(2)O15	n	1.84465	C14-C16	σ*	0.05943	18.69	0.62	0.099
LP(2)O20	n	1.88876	C19-O23	σ*	0.07655	17.47	0.55	0.089
LP(2)O23	n	1.83011	C19-O20	σ*	0.04686	10.20	0.63	0.074
LP(2)O23	n	1.83011	C21-C22	π*	0.14082	<b>31.04</b>	0.35	0.093
LP(2)O25	n	1.92061	C4-C7	σ*	0.05030	5.27	0.64	0.052
LP(1)O28	n	1.95403	C60-C62	σ*	0.05935	6.44	0.91	0.069
LP(2)O28	n	1.80819	C2-C3	σ*	0.02518	5.12	0.71	0.056
LP(2)O28	n	1.80819	C60-O61	π*	0.20037	<b>39.92</b>	0.35	0.105
LP(2)O61	n	1.84490	O28-C60	σ*	0.10921	<b>35.28</b>	0.61	0.132
LP(2)O61	n	1.84490	C60-C62	σ*	0.05935	18.86	0.62	0.099

DCLD								
Donor(i)	Type	ED/e	Acceptor(j)	Type	ED/e	E(2) <sup>a</sup>	E(j)-E(i) <sup>b</sup>	F(i,j) <sup>c</sup>
C3 - O18	σ	1.97346	O18 - C19	σ*	0.02370	5.05	0.93	0.061
C11 - C20	σ	1.97623	C21 - C25	σ*	0.02152	5.88	0.99	0.068
O18 - C19	σ	1.97752	C3 - O18	σ*	0.04797	5.57	0.91	0.064
C11 - O23	σ	1.97642	C22 - O27	σ*	0.05534	5.34	1.01	0.066
LP(2)O17	n	1.95745	C16 - H46	σ*	0.02491	5.75	0.75	0.059
LP(2)O18	n	1.92189	C3 - C4	σ*	0.04802	5.16	0.64	0.052
LP(2)O18	n	1.92189	C2 - C3	σ*	0.03155	5.18	0.69	0.054
LP(2)O23	n	1.92295	C22 - H29	σ*	0.05194	8.97	0.74	0.073
LP(2)O27	n	1.85883	C25 - C26	π*	0.12391	<b>23.83</b>	0.38	0.086

a E(2) means energy of hyperconjugative interactions (stabilization energy in Kcal/mol)

b Energy difference between donor and acceptor i and j NBO orbitals in a.u.

c F(i,j) is the Fock matrix elements between i and j NBO orbitals in a.u.

#### 4.6 Non Linear Optical Analysis

In order to investigate the relationship between molecular structure and NLO response, first hyperpolarizability ( $\beta_{\text{total}}$  (esu)) and related properties such as polarizability ( $\alpha$ ), and total dipole moment ( $\mu$ ) have been calculated using B3LYP/6-31G (d, p) based on the finite-field approach. First hyperpolarizability is a third rank tensor and can be described by a 3 x 3 x 3 matrix. The 27 components of the 3 dimensional matrixes can be reduced to 10 components due to the Kleinman symmetry.<sup>[61]</sup> The intermolecular interactions involving the non-bonded type dipole-dipole interactions are determined with the help of dipole moment of a molecule means stronger the dipole moment, stronger will be the intermolecular interactions. All NLO parameters are calculated according to the equations follows:

$$\mu_{\text{tot}} = (\mu_x^2 + \mu_y^2 + \mu_z^2)^{1/2} \quad (11)$$

$$\alpha_{\text{tot}} = 1/3(\alpha_{xx} + \alpha_{yy} + \alpha_{zz}) \quad (12)$$

$$\langle \beta \rangle = [(\beta_{xxx} + \beta_{yyy} + \beta_{zzz})^2 + [(\beta_{yyy} + \beta_{yzz} + \beta_{yxx})^2 + [(\beta_{zzz} + \beta_{zxx} + \beta_{zyy})^2]]^{1/2} \quad (13)$$

If any molecule shows large value of the polarizability and hyperpolarizability it means there is a significant delocalization of charge in that molecule. The values of the dipole moment ( $\mu$ ), polarizability ( $\alpha$ ), first hyperpolarizability ( $\beta$ ) are mentioned in **Table 7**. It is clear from the **Table 7** that the **DCLD** compound shows the larger value of polarizability ( $\alpha$ ) equal to 41.6245 esu and hyperpolarizability ( $\beta$ ) equal to 2.92775 esu in comparison to **CLD** which showed the lower value of of polarizability ( $\alpha$ ) is equal to 37.9883 esu and hyperpolarizability ( $\beta$ ) equal to 0.31182 esu. (Gaussian 09 output are reported in atomic unit (a.u.) so these values are converted into electrostatic unit (esu) using converting factors as (for ( $\alpha$ ): 1 a.u. = 0.1482 x 10<sup>-24</sup> esu; for  $\beta_{\text{total}}$ : 1 a.u. = 0.008639 x 10<sup>-30</sup> esu).

**Table 7.** Dipole Moment  $\mu$ , Polarizability  $\alpha_{tot}$  ( $10^{-24}$  esu) and first order static hyperpolarizability  $\beta_{tot}$  ( $10^{-30}$ ) data for **CLD** and **DCLD** calculated at DFT/B3LYP /6-31G(d,p) level of theory

Dipole moment			Hyperpolarizability		
CLD	DCLD		CLD	DCLD	
$\mu_x$	6.5561	0.5073			
$\mu_y$	-0.6352	-2.1743	$\beta_{xxx}$	33.3304	234.398
$\mu_z$	0.7182	3.0365	$\beta_{xyy}$	27.1601	77.1294
$\mu$	<b>6.6258</b>	<b>3.7690</b>	$\beta_{xyy}$	-3.07176	-28.7653
Polarizability			$\beta_{yyy}$	-41.1772	-41.1772
CLD	DCLD				
$\alpha_{xx}$	310.893	304.844	$\beta_{xxz}$	8.66946	60.2729
$\alpha_{xy}$	-0.778433	-7.12231	$\beta_{xyz}$	9.97575	0.202684
$\alpha_{yy}$	239.239	281.945	$\beta_{yyz}$	-75.5409	14.0859
$\alpha_{xz}$	-6.32552	4.12070	$\beta_{xzz}$	5.46886	41.2288
$\alpha_{yz}$	3.12718	5.28375	$\beta_{yzz}$	9.00521	32.0298
$\alpha_{zz}$	218.862	255.812	$\beta_{zzz}$	65.7940	34.2992
$(\alpha)$	<b>37.9883</b>	<b>41.6245</b>	$\beta_{total}(esu)$	<b>0.31182</b>	<b>2.92775</b>

#### 4.7 Local Reactivity Descriptors

Fukui function (FF), local softness ( $S_k$ ) and local electrophilicity index ( $\omega_k$ ) are the tools mostly used in computational chemistry for chemical reactivity and site selectivity of the compounds. Using Hirshfield population analysis of neutral, cation and anion state of molecule, Fukui Functions are calculated by using the following equations:

$$f_k^+ = [q(N+1) - q(N)] \text{ for nucleophilic attack} \quad (14)$$

$$f_k^- = [q(N) - q(N-1)] \text{ for electrophilic attack} \quad (15)$$

$$f_k^0 = 1/2[q(N+1) - q(N-1)] \text{ for radical attack} \quad (16)$$

Where N, N-1, N+1 are total electrons present in neutral, anion and cation state of molecule respectively. Local softness ( $S_k$ ) functions are calculated according to the following equations:

$$S_k^+ = S f_k^+, S_k^- = S f_k^-, S_k^0 = S f_k^0 \quad (17)$$

$$S_k^+ = S f_k^+, S_k^- = S f_k^-, S_k^0 = S f_k^0 \quad (18)$$

Selected Fukui functions, local softness and local electrophilicity indices for **CLD** and **DCLD** are listed in **Table 8**. In **CLD** maximum value of  $f_k^+$ ,  $s_k^+$ ,  $\omega_k^+$  are 0.291054, 0.047331 and 0.40955 respectively for atomic site C21, hence it is the most prone site for nucleophilic attack than other sites listed in **Table 8**. Maximum values of  $f_k^-$ ,  $s_k^-$ ,  $\omega_k^-$  are 0.094328, 0.01534, 0.132731 and 0.122306, 0.019889, 0.1721 for atomic site O25 and C60 respectively hence these sites are more prone for the electrophilic attack in **CLD** compound. For the **DCLD** compound, it is also clear from **Table 8** that the maximum value of  $f_k^+$ ,  $s_k^+$ ,  $\omega_k^+$  are 0.096218, 0.014529, 0.112094 respectively for atomic site C20 hence it is the most prone site for nucleophilic attack and maximum values of  $f_k^-$ ,  $s_k^-$ ,  $\omega_k^-$  are 0.630315, 0.095178, 0.734317 for atomic site O17 respectively hence these sites are more prone for the electrophilic attack.

**Table 8.** Using Hirshfield population analysis: Fukui functions ( $f_k^+$ ,  $f_k^-$ ), Local softnesses ( $s_k^+$ ,  $s_k^-$ ) in eV, local electrophilicity indices ( $\omega_k^+$ ,  $\omega_k^-$ ) in eV for selected atomic sites of product

Atom no.	CLD			Fukui functions		Local softnesses		Local electrophilicity indices	
	Hirshfeld atomic charges			$f_{k+}$	$f_{k-}$	$s_k^+$	$s_k^-$	$\omega_k^+$	$\omega_k^-$
	$q_N$	$q_{N+1}$	$q_{N-1}$						
11C	0.20257	0.32334	0.27873	0.12077	-0.07617	0.01964	-0.01239	0.169939	-0.10718
17C	0.0077	0.13481	-0.0157	0.127112	0.023378	0.020671	0.003802	0.178863	0.032896
<b>21C</b>	-0.0364	0.25469	-0.144	<b>0.291054</b>	0.10761	<b>0.047331</b>	0.0175	<b>0.40955</b>	0.151421
22C	0.29925	0.51709	0.1656	0.217839	0.133651	0.035425	0.021734	0.306527	0.188064
12O	-0.4151	-0.4781	-0.4837	-0.06299	0.06865	-0.01024	0.011164	-0.08863	0.096599
14C	0.60078	0.59436	0.53812	-0.00642	0.062662	-0.00104	0.01019	-0.00903	0.088173
<b>25O</b>	-0.4181	-0.5166	-0.5124	-0.09851	<b>0.094328</b>	-0.01602	<b>0.01534</b>	-0.13862	<b>0.132731</b>
28O	-0.4168	-0.4971	-0.506	-0.08026	0.089183	-0.01305	0.014503	-0.11294	0.125492
<b>60C</b>	0.63197	0.60346	0.50967	-0.02851	<b>0.122306</b>	-0.00464	<b>0.019889</b>	-0.04012	<b>0.1721</b>
62C	-0.0164	0.05325	-0.0901	0.069695	0.073635	0.011334	0.011975	0.09807	0.103614
DCLD									
4C	-0.0685	-0.0111	-0.0099	0.057382	-0.05856	0.008665	-0.00884	0.06685	-0.06823
12C	-0.5858	-0.0113	-0.0362	0.574529	-0.54962	0.086754	-0.08299	0.669326	-0.6403
<b>20C</b>	-0.0097	0.08648	-0.0636	<b>0.096218</b>	0.053879	<b>0.014529</b>	0.008136	<b>0.112094</b>	0.062769
21C	0.01834	0.07522	-0.063	0.056886	0.081314	0.00859	0.012278	0.066272	0.094731
22C	0.55071	0.60941	0.47329	0.058699	0.077412	0.008864	0.011689	0.068384	0.090185
<b>17O</b>	0.39752	-0.2298	-0.2328	-0.62734	<b>0.630315</b>	-0.09473	<b>0.095178</b>	-0.73085	<b>0.734317</b>
25C	-0.0299	0.20567	-0.3746	0.235554	0.344689	0.035569	0.052048	0.27442	0.401563
26C	0.24857	0.51026	-0.0808	0.261689	0.329403	0.039515	0.04974	0.304868	0.383754

#### 4.8 UV-Visible Absorption Spectroscopy

All the theoretical calculations of UV–Visible absorption spectrum were done with the help of TD-DFT method using B3LYP/6-31G (d, p) basis set with Integral Equation Formalism Polarizable Continuum Model (IEFPCM) as solvent effect. The simulated UV data and related properties such as the electronic transitions, excitation energies, oscillator strength ( $f$ ), percentage contribution of probable transition and corresponding absorption wavelength have been listed in **Table 9** for **CLD** and **DCLD**. For **CLD** compound calculations by B3LYP functional predict one intense electronic transition at 170.96 nm with an oscillator strength  $f = 0.0646$  in chloroform which is in good agreement with the measured experimental data ( $\lambda_{\text{exp}} = 244$  nm in chloroform) as shown in **Fig. 6**. This electronic absorption corresponds to the transition from the molecular orbital HOMO -7 to the LUMO, HOMO -6 to the LUMO, HOMO -5 to the LUMO, HOMO -4 to the LUMO, HOMO -3 to the LUMO with 2.26 %, 7.09 %, 32.15 %, 3.57 % and 1.98 % contribution respectively.

For **DCLD** compound theoretical calculations predict one intense electronic transition at 203.49 nm with an oscillator strength  $f = 0.0659$  in chloroform which is in good agreement with the measured experimental data ( $\lambda_{\text{exp}} = 242$  nm in chloroform) as shown in **Fig. 7**. This electronic absorption corresponds to the transition from the molecular orbital HOMO to the LUMO, HOMO -1 to the LUMO, HOMO -2 to the LUMO with 1.93 %, 5.92 %, 39.60 % contribution respectively.

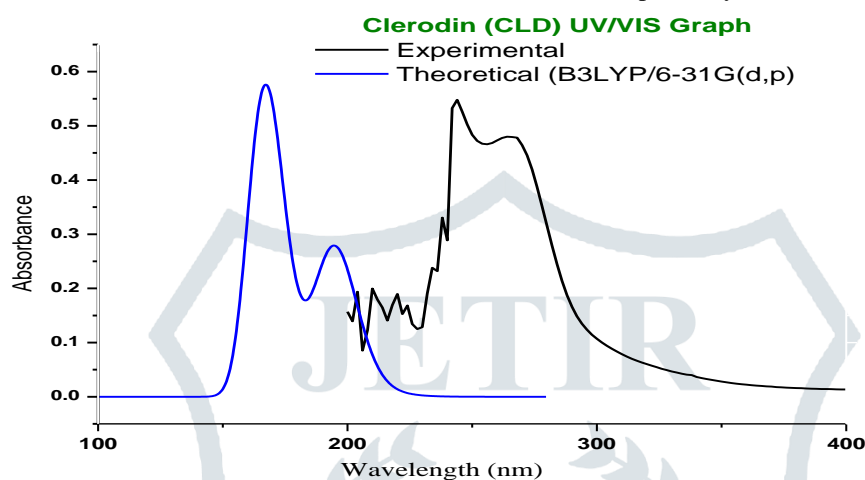


**Fig. 6.** Correlation graph between experimental and theoretical UV/VIS data of Absorption vs Wavelength of **CLD**

**Table 9.** Experimental and theoretical absorption wavelength  $\lambda$  (nm), excitation energies  $E$  (eV) of title compound using B3LYP functional and 631-G / (d, p) basis set

S. No.	Electronic transitions (molecular orbitals involved)	Excitation energies	Calculated $\lambda_{\text{max}}$ (in nm)	Oscillatory strength ( $f$ )	Percent contribution of probable transition	Observed $\lambda_{\text{max}}$ (in nm)
<b>CLD</b>						
1.	H-7 $\rightarrow$ L	8.081	170.96	0.0646	2.26	244
	H-6 $\rightarrow$ L	7.980			7.09	
	H-5 $\rightarrow$ L	7.875			32.15	
	H-4 $\rightarrow$ L	7.652			3.57	
	H-3 $\rightarrow$ L	7.608			1.98	
<b>DCLD</b>						
1.	H $\rightarrow$ L	11.27	203.49	0.0659	1.93	242
	H-1 $\rightarrow$ L	26.97			5.92	
	H-2 $\rightarrow$ L	77.78			39.60	

For **DCLD** compound theoretical calculations predict one intense electronic transition at 203.49 nm with an oscillator strength  $f = 0.0659$  in chloroform which is in good agreement with the measured experimental data ( $\lambda_{\text{exp}} = 242$  nm in chloroform) as shown in **Fig. 7**. This electronic absorption corresponds to the transition from the molecular orbital HOMO to the LUMO, HOMO -1 to the LUMO, HOMO -2 to the LUMO with 1.93 %, 5.92 %, 39.60 % contribution respectively.

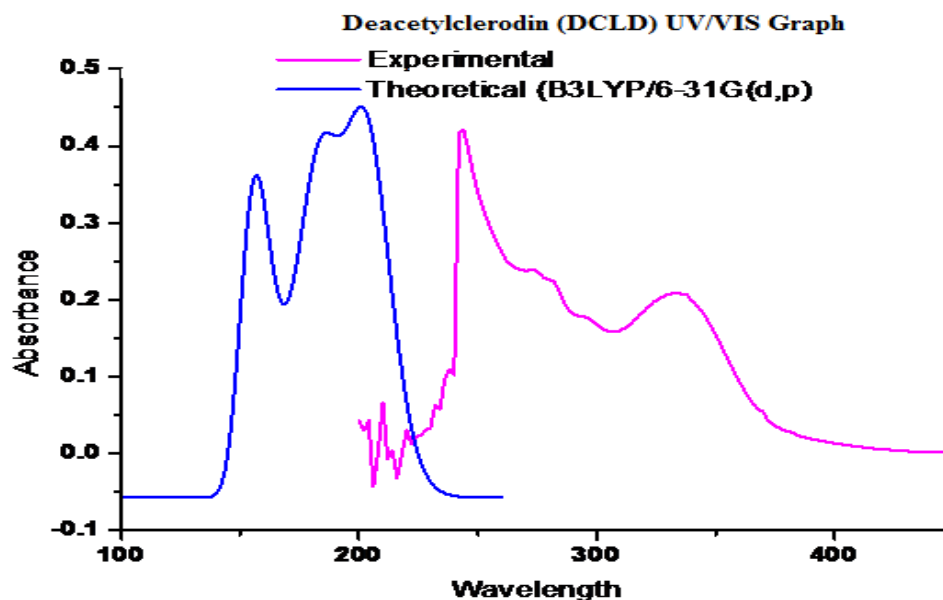


Fig. 7. Correlation graph between experimental and theoretical UV/VIS data of Absorption vs Wavelength of **DCLD**

#### 4.9 Vibrational Assignments

According to the molecular structure of **CLD** there are total 65 atoms which have total 189 normal modes of vibrations. All the 118 fundamental vibrations are IR active. The calculated harmonic vibrational frequencies at DFT (B3LYP) level using 6-31G (d, p) as the basis set have been compared with the experimental frequencies (FTIR) and are listed in **Table 10** and **11** for **CLD** and **DCLD** respectively. The correlation graph of calculated and experimental FTIR spectra of **CLD** and **DCLD** are given in **Fig. 8** and **9** respectively. Vibrational assignments are based on the observation of the animated modes in Gauss View. All the calculated vibrational frequencies are scaled by the factor of 0.9679.

In **CLD**, there are numbers of C-H group present in all the rings. The vibrational stretching frequency ( $\nu$ ) of C-H group is expected to occur in the region  $2900\text{--}3200\text{ cm}^{-1}$ . **Table 10** shows that the calculated vibrations are also found in this spectral region. For C-H stretching vibrations, intense bands are calculated at  $3149, 3041, 3012, 2932$  and  $2904\text{ cm}^{-1}$  which matches well with the experimental frequencies observed at  $3140, 3040, 2930$  and  $2931\text{ cm}^{-1}$  for **CLD** and calculated C-H stretching vibrations for **DCLD** are  $3072, 2970, 2929$  and  $2906\text{ cm}^{-1}$  which matches well with the experimental frequencies observed at  $2968.58, 2942.53$  and  $2846.49\text{ cm}^{-1}$  and  $2846.49\text{ cm}^{-1}$  matches well with the experimental frequencies observed at  $2968.58, 2942.53$  and  $2846.49\text{ cm}^{-1}$ . Other important stretching frequency in both compound is double bond stretching frequency which lies in the region of  $1600\text{--}1750\text{ cm}^{-1}$  corresponds to C=O, C=C, C=N, etc..The C=C bond is present between C21 and C22 shows calculated and experimental stretching frequencies at  $1629$  and  $1625\text{ cm}^{-1}$  respectively in **CLD**. In **DCLD**, C=C (between 25C and 26C) bond shows calculated and experimental stretching frequencies at  $1623$  and  $1619.31\text{ cm}^{-1}$  respectively. The **CLD** molecule has two carbonyl (C=O) group (between  $14\text{C} = 15\text{O}$  and  $60\text{C} = 61\text{O}$ ) which shows calculated and experimental stretching frequencies at  $1734$  and  $1731\text{ cm}^{-1}$  for  $14\text{C} = 15\text{O}$  and  $1741$  and  $1736\text{ cm}^{-1}$  for  $60\text{C} = 61\text{O}$  respectively. In **DCLD** molecule two hydroxyl group are present having corresponding calculated stretching frequencies at  $3682\text{ cm}^{-1}$  (17O-48 H),  $3666\text{ cm}^{-1}$  (38O-55 H) and experimental stretching frequencies at  $3462.37\text{ cm}^{-1}$  (17O-48 H),  $3364.96\text{ cm}^{-1}$  (38O-55 H) respectively. In **CLD** due to the deformation of ring R2, R4 and in whole molecule vibrations, the intense band is calculated at  $1271\text{ cm}^{-1}$  and  $1314\text{ cm}^{-1}$  respectively and which is in very good agreement with the experimental one that is,  $1372\text{ cm}^{-1}$ , and  $1388\text{ cm}^{-1}$ . In **DCLD** molecule many C-H deformation vibrations are calculated at  $1400, 1369, 1379$  and  $1280\text{ cm}^{-1}$ .

In both compounds many C-O bonds are also present which show different stretching frequencies in the region of  $1000\text{--}1250\text{ cm}^{-1}$  depending on the environment in which the C-O bond is present. In **CLD** the calculated C-O stretching vibrational frequencies observed at  $1217\text{ cm}^{-1}$  (60C - 28O),  $1206\text{ cm}^{-1}$  (14C - 12O),  $1076\text{ cm}^{-1}$  (19C - 20O),  $1059\text{ cm}^{-1}$  (11C - 12O),  $1052\text{ cm}^{-1}$  (3C - 28O) and  $1034\text{ cm}^{-1}$  (22C - 23O) which shows a good correlation with experimental C-O stretching vibrational frequencies observed at  $1288, 1272, 1238$  and  $1051\text{ cm}^{-1}$ . While in **DCLD** the calculated C-O stretching vibrational frequencies observed at  $1124\text{ cm}^{-1}$  (12C- 23O),  $1077\text{ cm}^{-1}$  (12C- 27O) and  $1063\text{ cm}^{-1}$  (16C- 17O). In **DCLD** the experimental C-O stretching vibrational frequencies observed at  $1135\text{ cm}^{-1}$ ,  $1103\text{ cm}^{-1}$ ,  $1053\text{ cm}^{-1}$ ,  $1037\text{ cm}^{-1}$ . An intense band due to butterfly motion in  $\text{CH}_3$  appears in the experimental spectrum at  $1471\text{ cm}^{-1}$ ,  $1453\text{ cm}^{-1}$  in **CLD** and **DCLD** respectively which matches well the peak at  $1472\text{ cm}^{-1}$ ,  $1433\text{ cm}^{-1}$  for **CLD** and  $1487\text{ cm}^{-1}$ ,  $1460\text{ cm}^{-1}$  for **DCLD** in the calculated spectrum. There are some frequencies in the lower region due to the torsion and mixed bending modes having appreciable IR intensity in calculated FTIR spectrum. Furthermore, the study of low frequency vibrations is of great significance, because it gives information on weak intermolecular interactions, which takes place in enzyme reactions. Knowledge of low frequency mode is also essential for the interpretation of the effect of electromagnetic radiation on biological systems [62].

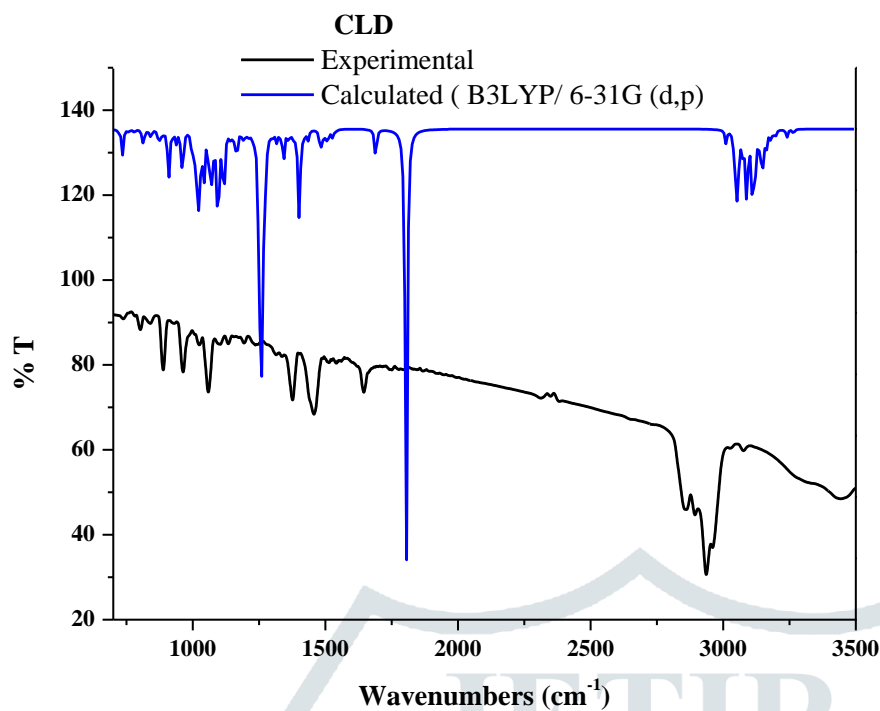


Fig. 8. Correlation graph of calculated and experimental FTIR spectra of **CLD**

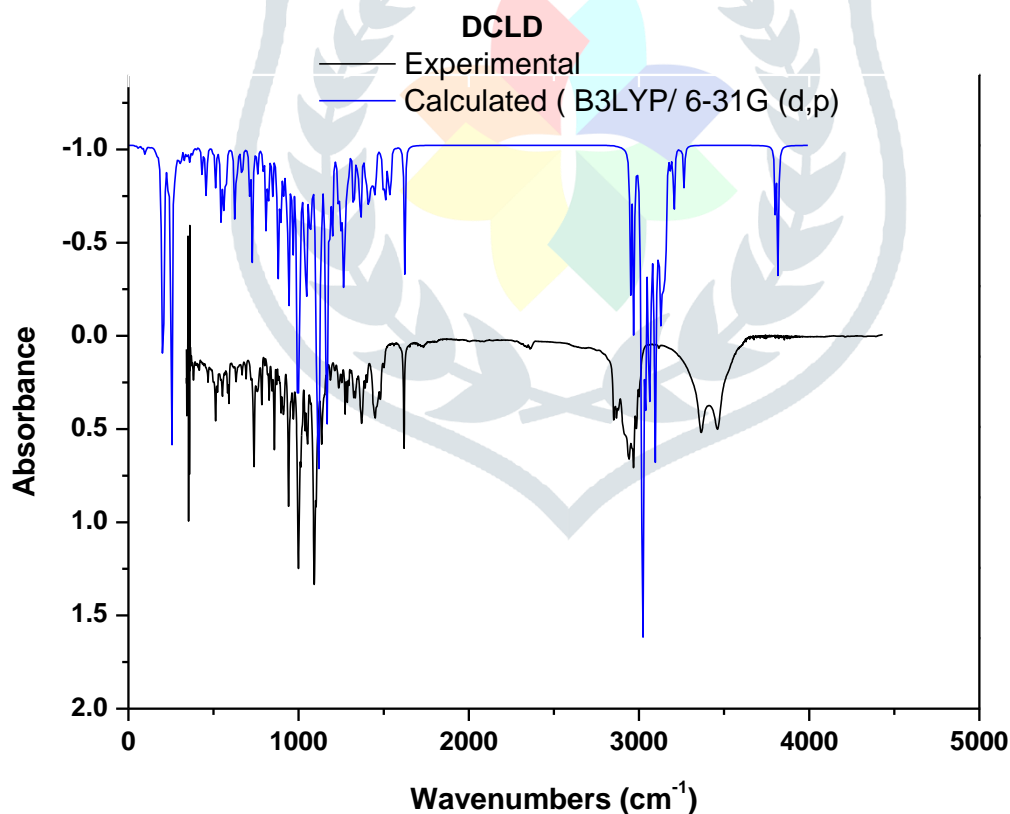


Fig. 9. Correlation graph of calculated and experimental FTIR spectra of **DCLD**

Table 10. Vibrational analysis of prominent modes of CLD at B3LYP/6-31G (d, p)

Calc. Freq. (cm <sup>-1</sup> ) (B3LYP/631G(d,p))	Scaled Freq. (cm <sup>-1</sup> )	Exp.	IR Int. (a.u.)	Assignments of vibrational modes
3264	3149.1072	3140	10.9986	$\nu$ =C-H (21C & 22C)
3239	3124.9872		15.04	$\nu_{as}$ CH <sub>2</sub> (26C)
3196	3083.5008		19.15	$\nu_{as}$ CH <sub>2</sub> (11C)
3181	3069.0288		10.69	$\nu_{as}$ CH <sub>3</sub> (62C)
3179	3067.0992		13.29	$\nu_{as}$ CH <sub>3</sub> (16C)
3164	3052.6272		17.56	$\nu_{as}$ CH <sub>3</sub> (24C)
3161	3049.7328		31.35	$\nu_{as}$ CH <sub>2</sub> (27C)
3152	3041.0496	3040	9.4	$\nu$ C-H (3C)
3149	3038.1552		63.53	$\nu_{as}$ CH <sub>2</sub> (10C)
3143	3032.3664		30.08	$\nu_{as}$ CH <sub>3</sub> (27C)
3139	3028.5072		32.56	$\nu_{as}$ CH <sub>2</sub> (17C)
3137	3026.5776		2.53	$\nu_{as}$ CH <sub>2</sub> (62C)
3122	3012.1056		75.99	$\nu$ C-H (19C)
3115	3005.352		74.63	$\nu_s$ CH <sub>2</sub> (26 C)
3110	3000.528		66.49	$\nu_{as}$ CH <sub>2</sub> (8C & 9C)
3107	2997.6336		69.29	$\nu_{as}$ CH <sub>2</sub> (24 C)
3088	2979.3024	2956	91.38	$\nu_s$ CH <sub>2</sub> (11C)
3085	2976.408	2936	53.66	$\nu_s$ CH <sub>2</sub> (17C)
3084	2975.4432		18.34	$\nu_{as}$ CH <sub>2</sub> (2 C)
3074	2965.7952		13.06	$\nu_s$ CH <sub>2</sub> (10C)
3058	2950.3584		52.67	$\nu_s$ CH <sub>2</sub> (8C & 9C)
3051	2943.6048		91.52	$\nu_s$ CH <sub>2</sub> (2C) + $\nu_s$ CH <sub>3</sub> (24C)
3039	2932.0272	<b>2930</b>	23.76	$\nu$ C-H (5C)
3010	2904.048	<b>2931</b>	31.51	$\nu$ C-H (1C)
1805	1741.464	1736	1000.56	$\nu_s$ C=O (60C- 61 O)
1798	1734.7104	1731	122.96	$\nu_s$ C=O (14C- 15 O)
1689	1629.5472	1625	75.65	$\nu$ C=C (21C & 22C)
1542	1487.7216		3.88	$\sigma$ - CH <sub>2</sub> (26CH <sub>2</sub> )
1526	1472.2848		4.26	BUTTERFLY CH <sub>3</sub> (27 C)
1525	1471.32		8.67	$\sigma$ - CH <sub>2</sub> (in whole molecule)
1486	1433.6928		7.4	BUTTERFLY CH <sub>3</sub> (62 C)
1435	1384.488		10.22	$\omega$ (CH <sub>2</sub> ) 26 C, 11C & 2C
1434	1383.5232		13.44	$\omega$ (CH <sub>3</sub> ) 27 C, 24 C
1402	1352.6496		99.8	$\omega$ (CH <sub>3</sub> ) 27 C, 24 C
1362	1314.0576	<b>1388</b>	12.34	(+) <i>def.</i> C-H (In whole molecule)
1318	1271.6064	<b>1372</b>	2.61	CH <i>def.</i> R2 R4
1262	1217.5776	1288	433.23	$\nu$ C-O (60C - 28O)
1250	1206	1272	354.54	$\nu$ C-O (14C - 12O)
1216	1173.1968		3.18	$\tau$ (CH <sub>2</sub> ) R2
1207	1164.5136		13.63	$\tau$ (CH <sub>2</sub> ) (In whole molecule)
1151	1110.4848		19.46	$\beta$ (CH)R3 R4
1116	1076.7168		180.04	$\nu$ C-O (19C - 20O)
1098	1059.3504		115.24	$\nu$ C-O (11C - 12O)
1091	1052.5968	1238	129.98	$\nu$ C-O (3C - 28O)
1072	1034.2656	1051	98.98	$\nu$ C-O (22C - 23O)
1042	1005.3216		102.56	$\beta$ (C-C-C) R3 R4
1020	984.096		151.92	$\beta$ (C-C-C) R1 R2
962	928.1376		75.71	$\beta$ (C-C-H) R1 R2
908	876.0384		126.07	$\gamma$ (CH) R1 R2 R3 R4
877	846.1296		24.75	$\rho$ (in whole molecule)

Table 11. Vibrational analysis of prominent modes of DCLD at B3LYP/6-31G(d, p)

Calc. Freq. (cm <sup>-1</sup> ) (B3LYP/631G(d,p))	Scaled Freq. (cm <sup>-1</sup> )	Exp.	IR (a.u.)	Int.	Assignments of vibrational modes
3817.26	3682.892	3462.37	56.81		$\nu$ (OH) 17O-48 H
3800	3666.24	3364.96	27.16		$\nu$ (OH) 38O-55 H
3265	3150.072	2968.58	19.02		$\nu$ =C-H (25C & 26C)
3205	3092.184	2942.53	32.01		$\nu_{as}$ CH <sub>2</sub> (19C)
3185	3072.888		6.88		$\nu$ C-H (12C)
3159	3047.803		26.79		$\nu_{as}$ CH <sub>3</sub> (13C)
3154	3042.979		16.74		$\nu_{as}$ CH <sub>2</sub> (2C)
3149	3038.155		38.51		$\nu_{as}$ CH <sub>2</sub> (20C)
3140	3029.472		28.82		$\nu_{as}$ CH <sub>2</sub> (8C)
3139	3028.507		40.26		$\nu_{as}$ CH <sub>2</sub> (6C)
3129	3018.859		39.76		$\nu_{as}$ CH <sub>3</sub> (12C)
3124	3014.035		42.6		$\nu_{as}$ CH <sub>2</sub> (16C)
3115	3005.352		38.13		$\nu_s$ CH <sub>2</sub> (19 C)
3099	2989.915		95.3		$\nu_{as}$ CH <sub>2</sub> (13C)
3094	2985.091		51.94		$\nu_s$ CH <sub>2</sub> (6 C)
3089	2980.267		41.68		$\nu_s$ CH <sub>2</sub> (20 C)
3079	2970.619		19.23		$\nu$ C-H (11C)
3067	2959.042		83.98		$\nu_{as}$ CH <sub>2</sub> (1C)
3060	2952.288		49.46		$\nu_s$ CH <sub>2</sub> (2 C)
3058	2950.358		59.47		$\nu_s$ CH <sub>3</sub> (12C)
3041	2933.957		81.17		$\nu_s$ CH <sub>3</sub> (13C)
3036	2929.133		33.43		$\nu$ C-H (9C)
3027	2920.45		63.74		$\nu_s$ CH <sub>2</sub> (16 C)
3023	2916.59		112.75		$\nu$ C-H (7C , 8C)
3019	2912.731		86.36		$\nu_s$ CH <sub>2</sub> (1C)
3013	2906.942		38.55		$\nu$ C-H (5C)
2969	2864.491		83.61		$\nu$ C-H (21C)
2950	2846.16		65.66		$\nu$ C-H ( 22 C)
1623	1565.87	1619.31	54.98		$\nu$ C=C (25C & 26C)
1573	1517.63		10.44		$\sigma$ - CH <sub>2</sub> (16CH <sub>2</sub> & 19CH <sub>2</sub> )
1542	1487.722		12.34		BUTTERFLY CH <sub>3</sub> (12 C)
1514	1460.707		10.09		$\sigma$ - CH <sub>2</sub> (6CH <sub>2</sub> , 2CH <sub>2</sub> & 1CH <sub>2</sub> )
1510	1456.848		10.35		BUTTERFLY CH <sub>3</sub> (13 C)
1507	1453.954		4.26		$\sigma$ - CH <sub>2</sub> (20C)
1452	1400.89		18.69		(+) <i>def.</i> C-H (bridge head 22C)
1443	1392.206		20.84		$\tau$ (CH <sub>2</sub> ) R4
1430	1379.664		1181		$\omega$ (CH <sub>3</sub> ) 12 C & 13C + CH <i>def.</i> (whole molecule)
1419	1369.051		18		CH <i>def.</i> R1 R2
1407	1357.474		3.94		$\tau$ (in whole molecule)
1327	1280.29		13.94		(+) <i>def.</i> C-H (BRIDGE HEAD 5C)
1268	1223.366		41.26		$\gamma$ (CH ) R3 R4
1264	1219.507		35.16		$\omega$ (CH <sub>2</sub> , OH) 16C & 17H
1245	1201.176		39.98		$\omega$ (OH) 30O
1199	1156.795		29.14		$\beta$ (C-C-H) in whole molecule
1166	1124.957	1135.16	102.54		$\nu$ C-O (12C- 23O) + $\square$ R2
1117	1077.682	1103.33	170.19		$\nu$ C-O (12C- 27O)+ $\square$ R1
1102	1063.21	1053.18	69.85		$\nu$ C-O (16C- 17O)+ $\square$ R4
1066	1028.477		31.73		$\beta$ (C-C-C) R3 R4
1044	1007.251		94.95		$\beta$ (C-C-C) R1 R2
995	959.976	1037.75	184.55		$\nu$ 26C- 27O + $\square$ R4
942	908.8416		64.91		$\beta$ (C-C-H) R3 R4
925	892.44		12.42		$\beta$ (C-C-H) R2 R4

## 5. CONCLUSION

In conclusion, the isolation and purification of clerodin (CLD) from *C. infortunatum* followed by the synthesis of deacetylclerodin (DCLD) from CLD was done. The comparative quantum chemical calculations, using DFT and QTAIM analysis, have been performed on CLD and DCLD to investigate their electronic and topological features in an attempt to elucidate their chemical reactivity. The calculated results show that reactivity descriptors based on DFT calculations i.e. ionization potential (*IP*), electron affinity (*EA*), electronegativity ( $\chi$ ), global electrophilicity index ( $\omega$ ) and global softness (*S*) consistently predict the higher chemical reactivity of DCLD over CLD. The chemically reactive sites are also clear from the HOMO-LUMO and MESP surface

map. The present work is important due to the competence of the bond path concept <sup>[63]</sup> and the theory of atoms-in-compound <sup>[64]</sup> in computational chemistry.

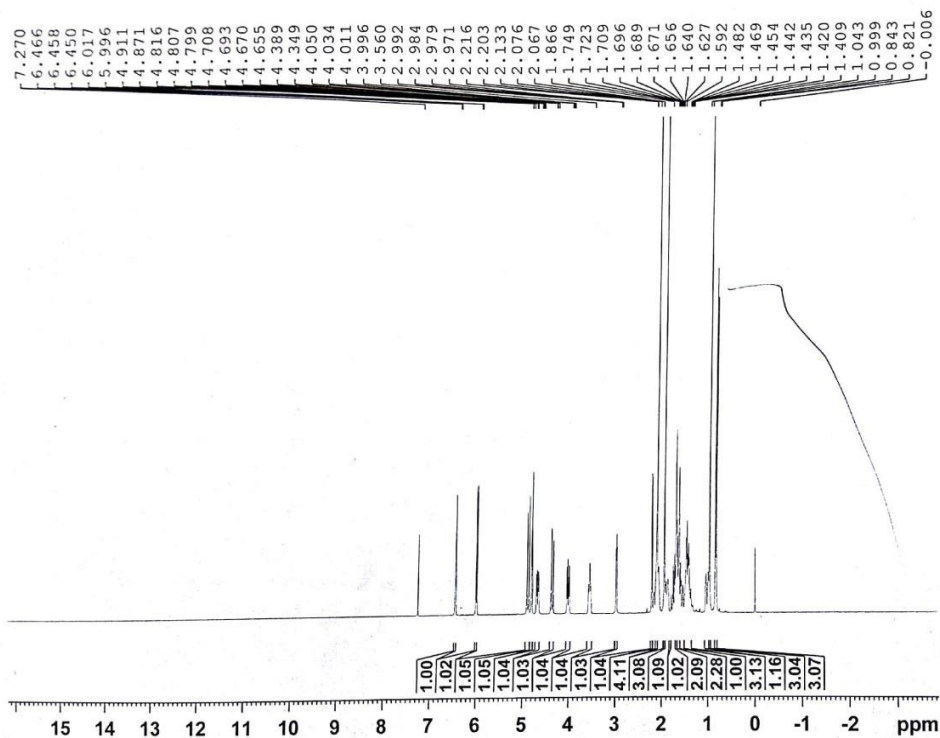
## 6. ACKNOWLEDGEMENT

The authors are thankful to the Department of Chemistry, University of Lucknow, Lucknow, UP for supporting UV, IR and NMR spectroscopic and computational facilities. Financial support from the University Grants Commission (UGC) and Council of Scientific and Industrial Research (CSIR), New Delhi is gratefully acknowledged. Ruchi Verma is thankful to UGC fellowship (RGNF) (file no.F117.1/2014-15/RGNF-2014-15-SC-UTT-78865), Reetu Sangwan is thankful to CSIR (File no. 09/107(0369)2014-EMR-I).

## REFERENCES

- [1] R. Li, S. L. Morris-Natschke, K. H. Lee, *Natural product reports*, **2016**, 33 (10), 1166-1226.
- [2] M. Rahmatullah, A. H. Mollik, N. Ahmed, Z. A. Bhuiyan, M. Hossain, N. K. Azam, S. Seraj, M. H. Chowdhury, F. Jamal, S. Ahsan, R. Jahan, *American-Eurasian journal of sustainable agriculture*, **2010**, 357-363.
- [3] S. Das, P. K. Haldar, G. Pramanik, R. B. Suresh, *Global J Pharmacol*, **2010**, 4(1) 48-50.
- [4] S. Sannigrahi, K. U. Mazumder, D. Pal, S. L. Mishra, *Pharmacognosy magazine*, **2009**, 5 (20), 394-399.
- [5] Kapoor LD. Handbook of Ayurvedic Medicinal Plants. 1st ed. New Delhi: CRC Press; **2001**, 124-5.
- [6] A. J. Modi, S. S. Khadabadi, S. L. Deore, *International Journal of PharmTech Research*, **2010**, 2 (1), 375-377.
- [7] D. Pal, S. Sannigrahi, U. K. Mazumder, *Indian J Exp Biol*, **2009**, 47,743-747.
- [8] S. Bhattacharya, Chiranjeev Vanaushadhi, IV, Kolkata: Ananda (In Bengali), **1981**.
- [9] S. Nandi, L. M. Lyndem, *Natural Product Research*, **2016**, 30 (5), 497-506.
- [10] B. V. Shetty, K. M. Kaveriappa, G. K. Bhat, Plant resources of Western Ghats and lowlands of Dakshina Kannada and Udupi districts. Pilikula Nisarga Dhama Society, Mangalore, India, **2002**, 159.
- [11] S. A. Punekar, P. Lakshminarasimhan, Flora of Anshi national park: Western Ghats-Karnataka, Biospheres Publication, Pune, India, **2011**, 370.
- [12] S. Yoganarasimhan, Medicinal plants of India – Tamilnadu. II. Bangalore: Cyber Media, **2000**.
- [13] S. S. Baid, *Asian J Comp Alt Med*, **2013**, 1(1), 1-8.
- [14] Y. Lallemand, Y. Six, L. Ricard, *Eur. J. Org. Chem.*, **2002**, 503–513.
- [15] T. K. Pal, S. Bhattacharyya, A. Dey, *Int.J.Curr.Microbiol.App.Sci*, **2014**, 3(4), 251-259.
- [16] S. K. Das, M. Masuda, A. Sakurai, M. Sakakibara, *Fitoterapia*, Medicinal uses of the mushroom *Cordyceps militaris*: current state and prospects, **2010**, 81 (8), 961-968.
- [17] V. K. Singh, Z. A. Ali, M. K. Siddiqui, *Int J Pharm*, **1997**, 35, 194–206.
- [18] A. N. Korpenwar, *DAV International Journal of Science*, **2012**, 1(2), 60-65.
- [19] S. K. Das, *Pop. Kheti*, **2014**, 2 (2), 93-99.
- [20] G. N. K. Kumari, J. Balachandran, S. Aravind, M. R. Ganesh, *J. Agric. Food Chem.* **2003**, 51, 1555-1559.
- [21] N. Ritsuo; K. Kunji; A. Takashi; K. Yasumasa, *Biochemical Systematics and Ecology*, **2004**, 32(1), 15-25.
- [22] S. Sharma, G. Brahmachari, B. Banerjee, K. Nurjamal, A. Kumar, A. K. Srivastava, N. Misra, S. K. Pandey, V. K. Rajnikant, Gupta, *J. Mol. Struct.* **2016**, 1118, 344-355.
- [23] A. K. Srivastava, S. K. Pandey, N. Misra, *Chem. Phys. Lett.* **2016**, 655–656, 71-75.
- [24] H. He, H. Chen, Y. Zheng, X. Zhang, X. Yao, Z. Yu, S. Zhang, *Aust. J. Chem.* **2013**, 66(11), 1342-1351.
- [25] T. Kageyama, S. Uneme, M. Takase, K. Nomura, T. Nishinaga, *Aust. J. Chem.* **2014**, 67(5), 722-728.
- [26] K. Geetha, T. N. Rekha, M. Umadevi, B. J. M. Rajkumar, G. V. Sathe, P. Vanelle, T. Terme, O. Khoumeri, *Aust. J. Chem.* **2015**, 69(1), 76-84.
- [27] E. Montiel, J. Cruz, N. Jayanthi, S. Berne's, T. Pandiyan, *Aust. J. Chem.* **2010**, 63(6), 965-977.
- [28] B. M. Alzoubi, R. Puchta, R. van Eldik, *Aust. J. Chem.* **2010**, 63(2), 236-244.
- [29] A. C. Tsipis, *RSC Adv.* **2014**, 4, 32504-32529.
- [30] H. Vovusha, B. Sanyal, *RSC Adv.* **2015**, 5, 67427-67434.
- [31] Y. Vesga, C. Diaza, F. E. Hernandez, *RSC Adv.* **2014**, 4, 60974-60986.
- [32] R. F. W. Bader, *Atoms in Compound: A Quantum Theory* (2nd edn) **1990** (Oxford: New York, NY).
- [33] R. F. W. Bader, *Chem. Rev.* **1991**, 91, 893-928.
- [34] M.J. Frisch, G.W. Trucks, H.B. Schlegel, G.E. Scuseria, M.A. Robb, J.R. Cheeseman, J.A. Montgomery, Jr., T. Vreven, K.N. Kudin, J.C. Burant, J.M. Millam, S.S. Iyengar, J. Tomasi, V. Barone, B. Mennucci, M. Cossi, G. Scalmani, N. Rega, G.A. Petersson, H. Nakatsuji, M. Hada, M. Ehara, K. Toyota, R. Fukuda, J. Hasegawa, M. Ishida, T. Nakajima, Y. Honda, O. Kitao, H. Nakai, M. Klene, X. Li, J.E. Knox, H.P. Hratchian, J.B. Cross, V. Bakken, C. Adamo, J. Jaramillo, R. Gomperts, R.E. Stratmann, O. Yazyev, A.J. Austin, R. Cammi, C. Pomelli, J.W. Ochterski, P.Y. Ayala, K. Voth, G.A. Morokuma, P. Salvador, J.J. Dannenberg, V.G. Zakrzewski, S. Dapprich, A.D. Daniels, M.C. Strain, O. Farkas, D.K. Malick, A.D. Rabuck, K. Raghavachari, J.B. Foresman, J.V. Ortiz, Q. Cui, A.G. Baboul, S. Clifford, J. Cioslowski, B.B. Stefanov, G. Liu, A. Liashenko, P. Piskorz, I. Komaromi, R.L. Martin, D.J. Fox, T. Keith, M.A. Al-Laham, C.Y. Peng, A. Nanayakkara, M. Challacombe, P.M.W. Gill, B. Johnson, W. Chen, Wong, M.W. Wong, C. Gonzalez, J.A. Pople, Gaussian 03, Revision C.02, Gaussian Inc., Wallingford, CT, **2004**.
- [35] M.J. Frisch, G.W. Trucks, H.B. Schlegel, G.E. Scuseria, M.A. Robb, J.R. Cheeseman, G. Scalmani, V. Barone, B. Mennucci, G.A. Petersson, H. Nakatsuji, M. Caricato, X. Li, H.P. Hratchian, A.F. Izmaylov, J. Bloino, G. Zheng, J.L. Sonnenberg, M. Hada, M. Ehara, K. Toyota, R. Fukuda, J. Hasegawa, M. Ishida, T. Nakajima, Y. Honda, O. KitÅ, H. Nakai, T. Vreven, J.A. Montgomery, Jr., J.E. Peralta, F. Ogliaro, M. Bearpark, J.J. Heyd, E. Brothers, K.N. Kudin, V.N. Staroverov, R. Kobayashi, J. Normand, K. Raghavachari, A. Rendell, J.C. Burant, S.S. Iyengar, J. Tomasi, M. Cossi, N. Rega, J.M. Millam, M. Klene, J.E. Knox, J.B. Cross, V. Bakken, C. Adamo, J. Jaramillo, R. Gomperts, R.E. Stratmann, O. Yazyev, A.J. Austin, R. Cammi, C. Pomelli, J.W. Ochterski, R.L. Martin, K. Morokuma, V.G. Zakrzewski, G.A. Voth, P. Salvador, J.J.

- Dannenber, S. Dapprich, A.D. Daniels, O. Farkas, J.B. Foresman, J.V. Ortiz, J. Cioslowski, D.J. Fox, Gaussian Inc., Wallingford, CT, **2009**.
- [36] Computer program Gauss View 3.09, Ver. 2, Gaussian Inc., Pittsburgh, PA.
- [37] E. Frisch, H.P. Hratchian, R.D. Dennington II, T.A. Keith, J. Millam with B. Nielsen, A. J. Holder, J. Hiscocks. Gaussian, Inc. GaussView Version 5.0.8, **2009**.
- [38] P. M. Viruela, R. Viruela, E. Orti', J.L. Bre'das, *J. Am. Chem. Soc.*, **1997**, 119, 1360-1369.
- [39] S. Shahab, R. Kumar, M. Darroudi, M. Y. Borzehandani, *J. Mol. Struct.* **2015**, 1083, 198-203.
- [40] A. Irfan, A. G. Al-Sehemi, A. Kalam, *J. Mol. Struct.*, **2013**, 1049, 198-204.
- [41] A. Irfan, R. Jin, A.G. Al-Sehemi, A. M. Asiri, *Spectrochim. Acta, Part A*, **2013**, 110, 60-66.
- [42] A. Irfan, A. G. Al-Sehemi, S. Muhammad, *Synthetic Metals*, **2014**, 190, 27-33.
- [43] S. M. Soliman, R. Assem, M. A.M. Abu-Youssef, T. S. Kassem, *J. Mol. Struct.* **2015**, 1085, 126-136.
- [44] A. Irfan, A. G. Al-Sehemi, M. Sultan Al-Assiri, *Computational and Theoretical Chemistry*, **2014**, 1031, 76-82.
- [45] W. Amamou, N. Elleuch, H. Feki, N. Chniba-boudjada, F. Zouari, *J. Mol. Struct.*, **2015**, 1083, 168-174.
- [46] A. D. Becke, *J. Chem. Phys.*, **1993**, 98, 5648-5652.
- [47] C. T. Lee, W.T. Yang, R.G.B. Parr, *Phys. Rev.*, **1988**, 37, 785-790.
- [48] R. F. W. Bader, *Atoms in Compound: A Quantum Theory (2nd edn)*, **1990** (Oxford: New York, NY).
- [49] S. K. Pandey, M. F. Khan, S. Awasthi, R. Sangwan, S. Jain, *Australian Journal of Chemistry*, **2016**, 70(3) 328-337.
- [50] I. Rozas, I. Alkorta, J. Elguero, *J. Am. Chem. Soc.* **2000**, 122(45), 11154-11161.
- [51] L. J. Guo, C.X. Wei, J.H. Jia, L.M. Zhao, Z.S. Quan, *Eur. J. Med. Chem.*, **2009**, 44 954-958.
- [52] A. Zarghi, R. Ghodsi, E. Azizi, B. Daraie, M. Hedayati, O.G. Dadrass, *Bioorg. Med. Chem.*, **2009**, 17, 5312-5317.
- [53] S. Bawa, S. Kumar, S. Drabu, R. Kumar, *Pharm. Bioallied Sci.*, **2010**, 2, 64-71.
- [54] Y. Saito, N. Yamada, T. Teramoto, H. Itakura, Y. Hata, N. Nakaya, H. Mabuchi, M. Tushima, J. Sasaki, N. Ogawa, Y.A. Goto, *Atherosclerosis*, **2002**, 162, 373-379.
- [55] S. Zhao, W. Zhou, J. liu, *Bioorg. Med. Chem.*, **2009**, 17, 7915-7923.
- [56] G. R. Green, J. M. Evans, A. K. Vong, A. R. Katritzky, C. W. Rees, E. F. V. Scriven, Eds., **1995**, 5, p. 469, Pergamon Press, Oxford, UK.
- [57] F. M. Abdelrazek, P. Metz, O. Kataeva, A. Jager, S. F. El-Mahrouky, *Arch. Pharm.*, **2007**, 340, 543-548.
- [58] L. Bonsignore, G. Loy, D. Secci, A. Calignano, *Eur. J. Med. Chem.*, **1993**, 28, 517-520.
- [59] J. Bevan Ott. J.Boerio-Goates, *Calculations from statistical Thermodynamics*, Academic Press, **Publication**, San Diego, Calif, Elsevier, **2000**.
- [60] D. Sajan, L. Josepha, N. Vijayan, M. Karabacak, *Spectrochim. Acta, Part A.*, **2011**, 81, 85-98.
- [61] R. P. Singh, R. Kant, K. Singh, S. Sharma, A. Sethi, *J. Mol. Structure*, **2015**, 1095, 125-134.
- [62] A. K. Pandey, A. K. Bajpai, A. Kumar, M. Pal, V. Baboo and A. Dwivedi, *J. Theoretical Chem.*, **2014**, 4, 64-69.
- [63] R. F. W. Bader, *Atoms in Compound: A Quantum Theory (2nd edn)*, **1990** (Oxford: New York, NY).
- [64] R. F. W. Bader, *Chem. Rev.* **1991**, 91, 893-928.
- [65] Petko I. Bozov, Yoana P. georgiveva, Rumen D. mladenov Di Terpenoids with neo-Clerodane Skeleton from *Scutellaria Altissima* ANNUAL of SOFIA university "ST. KLIMENT OHRIDSKI" Faculty of Chemistry and Pharmacy **2014**, 106, 53-55.
- [66] Barton, Cheung, Cross, Jackman, and Martin-Smith, *Proc. Chem. Soc.*, **1961**, 76, 5061.



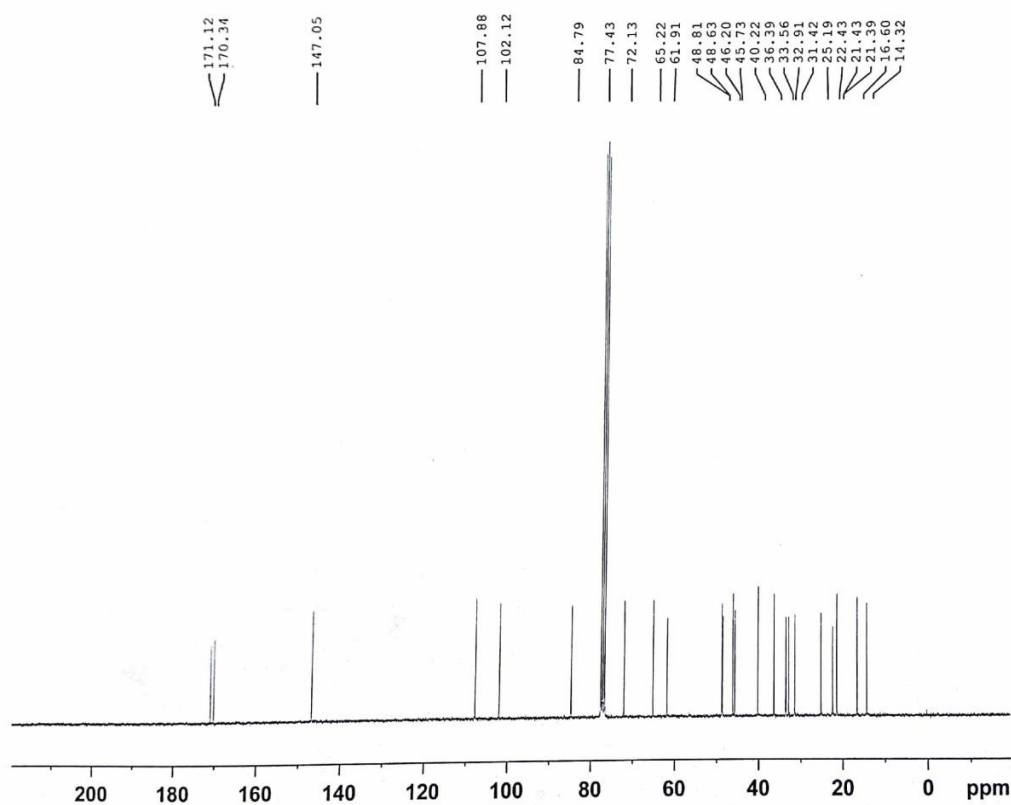
```
Current Data Parameters
NAME      Dec04-2015
EXPNO    30
PROCNO   1

F2 - Acquisition Parameters
Date_    20151204
Time     17.08
INSTRUM spect
PROBHD   5 mm PABBO BB-
PULPROG zg30
TD       65536
SOLVENT  CDCl3
NS       64
DS       2
SWH      6009.615 Hz
FIDRES   0.091699 Hz
AQ       5.4525952 sec
RG       157.27
DW       83.200 usec
DE       6.50 usec
TE       294.4 K
D1       1.00000000 sec
TD0      1

===== CHANNEL f1 =====
SFO1     300.2618542 MHz
NUC1     1H
P1       13.45 usec
PLW1     8.89999962 W

F2 - Processing parameters
SI       65536
SF       300.2600044 MHz
WDW      EM
SSB      0
LB       0.30 Hz
GB       0
PC       1.00
```

Fig S1. <sup>1</sup>H NMR Spectra of Clerodin (CLD)



```
Current Data Parameters
NAME      Dec04-2015
EXPNO    31
PROCNO   1

F2 - Acquisition Parameters
Date_    20151204
Time     19.22
INSTRUM spect
PROBHD   5 mm PABBO BB-
PULPROG zgpg30
TD       65536
SOLVENT  CDCl3
NS       2048
DS       4
SWH      18028.846 Hz
FIDRES   0.275098 Hz
AQ       1.8175317 sec
RG       199.93
DW       27.733 usec
DE       6.50 usec
TE       295.3 K
D1       2.00000000 sec
D11      0.03000000 sec
TD0      1

===== CHANNEL f1 =====
SFO1     75.5079867 MHz
NUC1     13C
P1       9.50 usec
PLW1     34.00000000 W

===== CHANNEL f2 =====
SFO2     300.2612010 MHz
NUC2     1H
CPDPRG[2] waltz16
PCPD2    90.00 usec
PLW2     8.89999962 W
PLW12    0.19877000 W
PLW13    0.16100000 W

F2 - Processing parameters
SI       32768
SF       75.5004240 MHz
WDW      EM
SSB      0
LB       1.00 Hz
GB       0
PC       1.40
```

Fig S2. <sup>13</sup>C NMR Spectra of Clerodin (CLD)

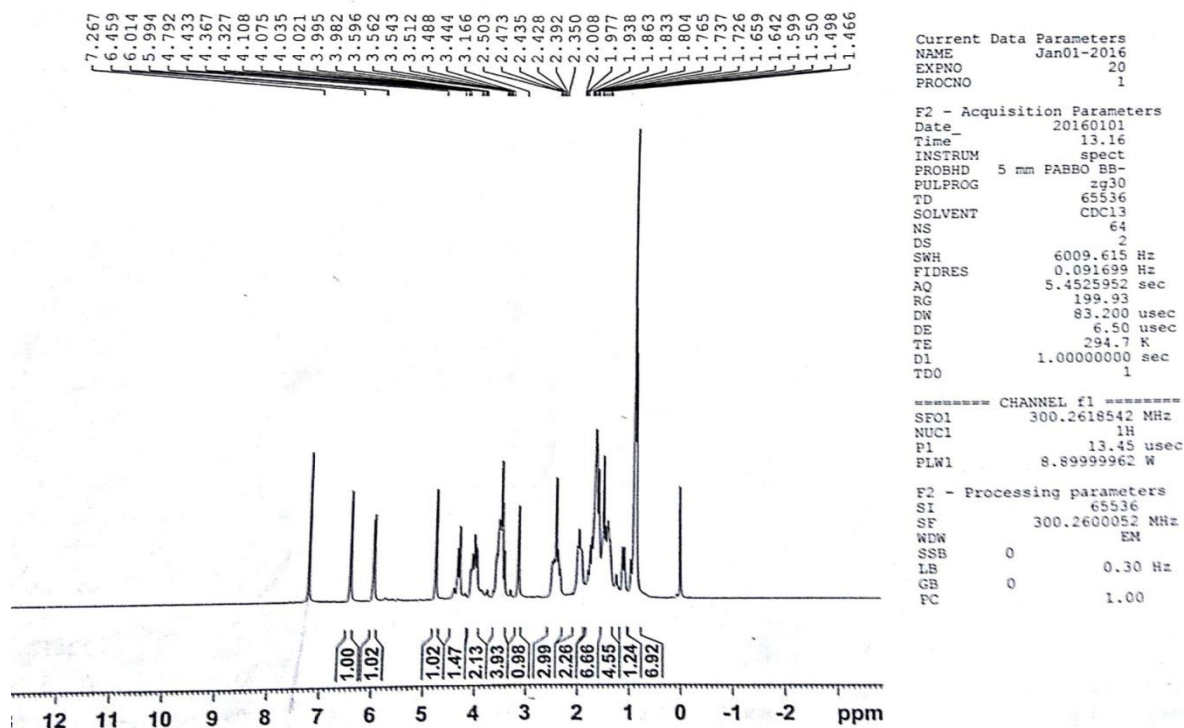


Fig S3. <sup>1</sup>H NMR Spectra of deacetylclerodin (DCLD)

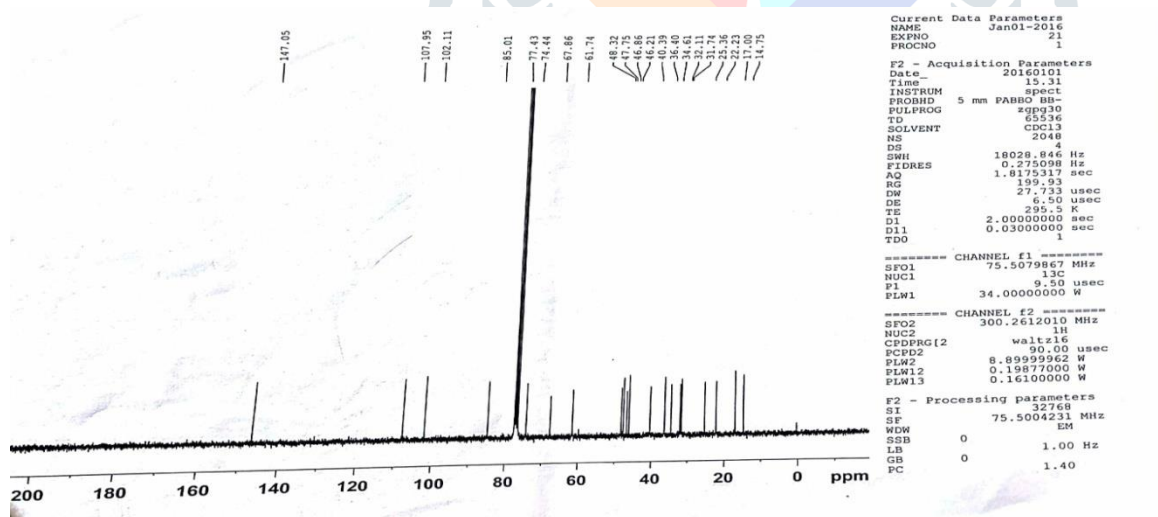


Fig S4. <sup>13</sup>C NMR Spectra of deacetylclerodin (DCLD)